Keisei Fujimori participated in the performance of the research

Kazuhiko Igarashi contributed to the analysis

Noriaki Ohuchi participated in the writing of the paper

Susumu Satomi participated in the writing of the paper

Masafumi Goto participated in the research design, the performance of the research, and the writing of the paper

Copyright © 2013 Cognizant Communication Corporation

References

1. Antonioli, B.; Fermo, I.; Cainarca, S.; Marzorati, S.; Nano, R.; Baldissera, M.; Bachi, A.; Paroni, R.; Ricordi, C.; Bertuzzi, F. Characterization of collagenase blend enzymes for human islet transplantation. Transplantation 84:1568-1575; 2007.

2. Bayne, K. Revised Guide for the Care and Use of Laboratory Animals available. American Physiological Society. Physiologist 39:199, 208-111; 1996.

3. Bedossa, P.; Lemaigre, G.; Bacci, J.; Martin, E. Quantitative estimation of the collagen content in normal and pathologic pancreas tissue. Digestion 44:7-13; 1989.

4. Bond, M. D.; Van Wart, H. E. Characterization of the individual collagenases from Clostridium histolyticum. Biochemistry (Mosc). 23:3085-3091; 1984.

5. Bond, M. D.; Van Wart, H. E. Purification and separation of individual collagenases of Clostridium histolyticum using red dye ligand chromatography. Biochemistry (Mosc). 23:3077-3085; 1984.

6. Bond, M. D.; Van Wart, H. E. Relationship between the individual collagenases of Clostridium histolyticum: evidence for evolution by gene duplication. Biochemistry (Mosc). 23:3092-3099; 1984.

7. Brandhorst, D.; Huettler, S.; Alt, A.; Raemsch-Guenther, N.; Kurfuerst, M.; Bretzel, R. G.; Brandhorst, H. Adjustment of the ratio between collagenase class II and I improves islet isolation outcome. Transplant. Proc. 37:3450-3451; 2005.

8. Brandhorst, H.; Friberg, A.; Andersson, H. H.; Felldin, M.; Foss, A.; Salmela, K.; Lundgren, T.; Tibell, A.; Tufveson, G.; Korsgren, O.; Brandhorst, D. The importance of tryptic-like activity in purified enzyme blends for efficient islet isolation. Transplantation 87:370-375; 2009.

9. Brandhorst, H.; Raemsch-Guenther, N.; Raemsch, C.; Friedrich, O.; Huettler, S.; Kurfuerst, M.; Korsgren, O.; Brandhorst, D. The ratio between collagenase class I and class II influences the efficient islet release from the rat pancreas. Transplantation 85:456-461; 2008.

10. French, M. F.; Bhown, A.; Van Wart, H. E. Identification of Clostridium histolyticum collagenase hyperreactive sites in type I, II, and III collagens: lack of correlation with local triple helical stability. J. Protein Chem. 11:83-97; 1992.

11. French, M. F.; Mookhtiar, K. A.; Van Wart, H. E. Limited proteolysis of type I collagen at hyperreactive sites by class I and II Clostridium histolyticum collagenases: complementary digestion patterns. Biochemistry (Mosc). 26:681-687; 1987.

12. Goto, M.; Eich, T. M.; Felldin, M.; Foss, A.; Kallen, R.; Salmela, K.; Tibell, A.; Tufveson, G.; Fujimori, K.; Engkvist, M.; Korsgren, O. Refinement of the automated method for human islet

isolation and presentation of a closed system for in vitro islet culture. Transplantation 78:1367-1375; 2004.

13. Goto, M.; Holgersson, J.; Kumagai-Braesch, M.; Korsgren, O. The ADP/ATP ratio: A novel predictive assay for quality assessment of isolated pancreatic islets. Am. J. Transplant. 6:2483-2487; 2006.

14. Huang, Z. H.; Shen, T.; Wu, J.; Gage, D. A.; Watson, J. T. Protein sequencing by matrix-assisted laser desorption ionization-postsource decay-mass spectrometry analysis of the N-Tris(2,4,6-trimethoxyphenyl)phosphine-acetylated tryptic digests. Anal. Biochem. 268:305-317; 1999.

15. Hughes, S. J.; Clark, A.; McShane, P.; Contractor, H. H.; Gray, D. W.; Johnson, P. R. Characterisation of collagen VI within the islet-exocrine interface of the human pancreas: implications for clinical islet isolation? Transplantation 81:423-426; 2006.

16. Kaddis, J. S.; Danobeitia, J. S.; Niland, J. C.; Stiller, T.; Fernandez, L. A. Multicenter analysis of novel and established variables associated with successful human islet isolation outcomes. Am. J. Transplant. 10:646-656; 2010.

17. Kin, T.; Zhai, X.; Murdoch, T. B.; Salam, A.; Shapiro, A. M.; Lakey, J. R. Enhancing the success of human islet isolation through optimization and characterization of pancreas dissociation enzyme. Am. J. Transplant. 7:1233-1241; 2007.

18. Kin, T.; Zhai, X.; O'Gorman, D.; Shapiro, A. M. Detrimental effect of excessive collagenase class II on human islet isolation outcome. Transpl. Int. 21:1059-1065; 2008.

19. Lakey, J. R.; Warnock, G. L.; Rajotte, R. V.; Suarez-Alamazor, M. E.; Ao, Z.; Shapiro, A. M.; Kneteman, N. M. Variables in organ donors that affect the recovery of human islets of Langerhans. Transplantation 61:1047-1053; 1996.

20. Mallya, S. K.; Mookhtiar, K. A.; Van Wart, H. E. Kinetics of hydrolysis of type I, II, and III collagens by the class I and II Clostridium histolyticum collagenases. J. Protein Chem. 11:99-107; 1992.

21. Nano, R.; Clissi, B.; Melzi, R.; Calori, G.; Maffi, P.; Antonioli, B.; Marzorati, S.; Aldrighetti, L.; Freschi, M.; Grochowiecki, T.; Socci, C.; Secchi, A.; Di Carlo, V.; Bonifacio, E.; Bertuzzi, F. Islet isolation for allotransplantation: variables associated with successful islet yield and graft function. Diabetologia 48:906-912; 2005.

22. Perkins, D. N.; Pappin, D. J.; Creasy, D. M.; Cottrell, J. S. Probability-based protein identification by searching sequence databases using mass spectrometry data. Electrophoresis 20:3551-3567; 1999.

23. Ponte, G. M.; Pileggi, A.; Messinger, S.; Alejandro, A.; Ichii, H.; Baidal, D. A.; Khan, A.; Ricordi, C.; Goss, J. A.; Alejandro, R. Toward maximizing the success rates of human islet isolation: influence of donor and isolation factors. Cell Transplant. 16:595-607; 2007.

24. Ryan, E. A.; Lakey, J. R.; Rajotte, R. V.; Korbutt, G. S.; Kin, T.; Imes, S.; Rabinovitch, A.; Elliott, J. F.; Bigam, D.; Kneteman, N. M.; Warnock, G. L.; Larsen, I.; Shapiro, A. M. Clinical outcomes and insulin secretion after islet transplantation with the Edmonton protocol. Diabetes 50:710-719; 2001.

25. Sabek, O. M.; Cowan, P.; Fraga, D. W.; Gaber, A. O. The effect of donor factors on human islet yield and their in vivo function. Prog. Transplant. 16:350-354; 2006.

26. Saito, Y.; Goto, M.; Maya, K.; Ogawa, N.; Fujimori, K.; Kurokawa, Y.; Satomi, S. The influence of brain death on tissue factor expression in the pancreatic tissues and isolated islets in rats. Transplant. Proc. 41:307-310; 2009.

27. Shapiro, A. M.; Lakey, J. R.; Ryan, E. A.; Korbutt, G. S.; Toth, E.; Warnock, G. L.; Kneteman, N. M.; Rajotte, R. V. Islet transplantation in seven patients with type 1 diabetes mellitus using a glucocorticoid-free immunosuppressive regimen. N. Engl. J. Med. 343:230-238; 2000.

28. Shapiro, A. M.; Ricordi, C.; Hering, B. J.; Auchincloss, H.; Lindblad, R.; Robertson, R. P.; Secchi, A.; Brendel, M. D.; Berney, T.; Brennan, D. C.; Cagliero, E.; Alejandro, R.; Ryan, E. A.; DiMercurio, B.; Morel, P.; Polonsky, K. S.; Reems, J. A.; Bretzel, R. G.; Bertuzzi, F.; Froud, T.; Kandaswamy, R.; Sutherland, D. E.; Eisenbarth, G.; Segal, M.; Preiksaitis, J.; Korbutt, G. S.; Barton, F. B.; Viviano, L.; Seyfert-Margolis, V.; Bluestone, J.; Lakey, J. R. International trial of the Edmonton protocol for islet transplantation. N. Engl. J. Med. 355:1318-1330; 2006.

29. Van Deijnen, J. H.; Van Suylichem, P. T.; Wolters, G. H.; Van Schilfgaarde, R. Distribution of collagens type I, type III and type V in the pancreas of rat, dog, pig and man. Cell Tissue Res. 277:115-121; 1994.

30. Watanabe, T.; Yaegashi, H.; Koizumi, M.; Toyota, T.; Takahashi, T. Changing distribution of islets in the developing human pancreas: a computer-assisted three-dimensional reconstruction study. Pancreas 18:349-354; 1999.

31. Wennberg, L.; Song, Z.; Bennet, W.; Zhang, J.; Nava, S.; Sundberg, B.; Bari, S.; Groth, C. G.; Korsgren, O. Diabetic rats transplanted with adult porcine islets and immunosuppressed with cyclosporine A, mycophenolate mofetil, and leflunomide remain normoglycemic for up to 100 days. Transplantation 71:1024-1033; 2001.

32. Wolters, G. H.; Vos-Scheperkeuter, G. H.; Lin, H. C.; van Schilfgaarde, R. Different roles of class I and class II Clostridium histolyticum collagenase in rat pancreatic islet isolation. Diabetes 44:227-233; 1995.

Table 1. The PCR primers used in the study

Primers		Sequences	Restriction sites
colG-F		5′-ATGAAAAAAAATATTTTAAAGATTC-3′	-
colG-R		5′-CCggatccTAtctagaTACCCTTAACT-3′	BamHI, XbaI
lac-F		5′-CCGGCaagcttGCCCAATACGCAAACCG-3′	HindIII
lac-R		5′-AGCTGTTTCCTGTGTGAA-3′	-
His-F		5′-GCtctagaAAGCTTGCGGCCGCACTCGA-3′	XbaI
His-R		5′-CGggatccGGATATAGTTCCTCCT-3′	BamHI
colH-F		5′-ATGAAAAGGAAATGTTTATC-3′	-
colH-R		5′-CCggatccTAtctagaTACTGAACCTT-3′	BamHI, XbaI

PCR, polymerase chain reaction

Copyright © 2013 Cognizant Communication Corporation

Table 2. Characterization of blended enzyme components

Group	Enzyme components	Enzyme activity (U)							
		Azcoll		Pz-PLGPR		Azocasein		Bz-Arg-pNA	
Crude collagenase	Sigma collagenase type V	15.0		21.0		190.0		45.0	
Experimental group	Thermolysin	15.0	0.90	21.0	4.06	190.0	190.0	ND	ND
	ColG		13.98		0.97		ND		ND
	ColH		0.12		15.97		ND		ND

Pz-PLGPR, 4-phenylazobenzyloxycarbonyl-Pro-Leu-Gly-Pro-D-Arg; ColG, collagenase G; ColH, collagenase H; ND, not detected

Table 3. The effects of collagenase subtypes on the functions of isolated rat islets

	GH	H	p value
ADP/ATP	0.02 ± 0.01	0.02 ± 0.03	0.93
ATP/DNA	54.96 ± 9.85	52.21 ± 5.79	0.48
Insulin/DNA	1.12 ± 0.23	1.12 ± 0.33	0.99
AUC in the IPGTT	12,163 ± 2799	12,100 ± 5301	0.97
Kg value in the IPGTT	1.74 ± 0.52	1.68 ± 0.63	0.85

ADP, adenosine diphosphate; ATP, adenosine triphosphate; DNA, deoxyribonucleic acid; AUC, area under the curve; IPGTT, intraperitoneal glucose tolerance test

Copyright © 2013 Cognizant Communication Corporation

Table 4. MASCOT search result for mass analyses

Accession	Score1	Score2	Score3	Description
gi|149040500	1439	1239	1649	Pancreatic lipase
CBPA1_RAT		504	579	508 Carboxypeptidase A1
gi|149025754	334	312	327	rCG28529
gi|149048540	216	265	149	Carboxypeptidase B1
gi|149040503	214	185	214	Pancreatic lipase related protein 1
gi|149065178	182	125	93	Carboxypeptidase A2
gi|157836327	170	208	157	Chain A, Rat Annexin V Crystal Structure
gi|1708841		162	199	166 Pancreatic lipase-related protein 2
CO3A1_RAT		153	297	328 Collagen alpha-1(III) chain
gi|6978801		127	47	186 Chymotrypsin-like elastase family member 1 precursor
CO1A1_RAT		125	275	115 Collagen alpha-1(I) chain
VDAC1_RAT	120	116	153	Voltage-dependent anion-selective channel protein 1
gi|149052643	117	141	111	rCG33456
CTRB1_RAT		106	98	57 Chymotrypsinogen B
gi|157821559	96	72	93	Chymotrypsin-like elastase family member 3B precursor
ANXA2_RAT	95	-	-	Annexin A2
gi|56200	94	-	-	Unnamed protein product
PRDX4_RAT		77	58	56 Peroxiredoxin-4
gi|281371499	70	51	67	Collagen, type V, alpha 2 precursor
gi|149015740	70	48	-	rCG39189
SODM_RAT		69	64	31 Superoxide dismutase
TRY3_RAT	68	78	86	Cationic trypsin-3
gi|13386010		67	-	- 60S ribosomal protein L22-like 1

CELL TRANSPLANTATION The Regenerative Medicine Journal

THIL_RAT	65	97	71		Acetyl-CoA acetyltransferase
SYCN_RAT	59	58	113		Syncollin
TRY1_RAT	57	57	57		Anionic trypsin-1
gi|293341509	55	48	51		Epoxide hydrolase 1-like
GRP78_RAT		53	89	82	78 kDa glucose-regulated protein
gi|204570	53	-	-		Major beta-hemoglobin
gi|149030731	52	-	53		Proteasome subunit, beta type 4
gi|149051043	52	-	40		rCG62292
PHB_RAT	51	57	40		Prohibitin
EF1A1_RAT		49	59	42	Elongation factor 1-alpha 1
GATM_RAT		48	84	43	Glycine amidinotransferase
gi|2920827		48	49	-	Ribosomal protein S2
BCAT2_RAT		48	-	-	Branched-chain-amino-acid aminotransferase
MCCB_RAT		46	42	-	Methylcrotonoyl-CoA carboxylase beta chain
gi|77993298		45	66	65	Translocon-associated protein subunit alpha precursor
TMED2_RAT	45	-	42		Transmembrane emp24 domain-containing protein 2
gi|158749632	43	-	-		Lipoamide acyltransferase
CH10_RAT	42	-	34		10 kDa heat shock protein
ENPL_RAT	42	-	-		Endoplasmin
gi|55628	40	-	53		Unnamed protein product
gi|157822495	40	-	-		Ribosomal protein S6 kinase alpha-5
gi|293349448	39	44	-		Collagen alpha-6(VI) chain-like
CH60_RAT	36	-	-		60 kDa heat shock protein
gi|374253859	35	-	-		Copine-3
CTRC_RAT	34	-	-		Chymotrypsin-C
NUAK2_RAT	32	-	-		NUAK family SNF1-like kinase 2
gi|392342412	32	-	-		DBF4-type zinc finger-containing protein 2 homolog
NOX4_RAT		31	-	-	NADPH oxidase 4
gi|293341660	30	-	51		Transmembrane protease serine 11F-like
gi|149039207	29	-	-		Procollagen, type V, alpha 1
gi|300798499	29	-	-		AF4/FMR2 family member 3
gi|149057763	28	60	-		Voltage-dependent anion channel 3

gi|162287135	28	-	-		Brain-enriched guanylate kinase-associated protein
gi|157821129	27	-	-		E3 ubiquitin-protein ligase UHRF2
gi|149047850	26	-	-		rCG37751
RS23_RAT	23	-	-		40S ribosomal protein S23
gi|157819565	18	-	17		WW domain-binding protein 1
DHE3_RAT	-	84	78		Glutamate dehydrogenase 1
HBB1_RAT	-	61	62		Hemoglobin subunit beta-1
gi|9027561		-	57	49	Antiquitin
gi|281427229	-	57	-		Collagen, type VI, alpha 2 precursor
gi|169234844	-	54	57		Vesicular integral-membrane protein VIP36 precursor
DJB11_RAT		-	50	-	DnaJ homolog subfamily B member 11
gi|149055897	-	48	48		Branched chain aminotransferase 2
PCYOX_RAT	-	46	-		Prenylcysteine oxidase
gi|149046794	-	43	-		Similar to hypothetical protein, isoform CRA_a
ATPB_RAT	-	42	-		ATP synthase subunit beta
gi|293350771	-	41	-		IQ motif and SEC7 domain-containing protein 2-like
gi|109508309	-	41	-		40S ribosomal protein S20-like
RS7_RAT	-	40	-		40S ribosomal protein S7
gi|13786202		-	-	112	Voltage-dependent anion-selective channel protein 2
ZG16_RAT	-	-	66		Zymogen granule membrane protein 16
CATD_RAT	-	-	56		Cathepsin D
gi|149031025	-	-	49		Histocompatibility 13
DLDH_RAT	-	-	49		Dihydrolipoyl dehydrogenase
gi|293349510	-	-	48		SH3 and cysteine-rich domain-containing protein
gi|149063028	-	-	48		Malate dehydrogenase
STS_RAT	-	-	44		Steryl-sulfatase
PRDX1_RAT		-	-	44	Peroxiredoxin-1
RL31_RAT	-	-	43		60S ribosomal protein L31
gi|392346433	-	-	39		LOW QUALITY PROTEIN
gi|164663906	-	-	37		Protein disulfide-isomerase A2 precursor
gi|203033	-	-	36		F1-ATPase beta subunit
gi|254221096	-	-	35		Single Type I Collagen

gi|392355927	-	-	35	NCK-associated protein 5-like
PHB2_RAT	-	-	33	Prohibitin-2
gi|13751173		-	-	32 TA1 KET alpha protein
gi|602756	-	-	32	Gamma-glutamyl transpeptidase
gi|392341097	-	-	30	Laminin subunit beta-1
RIT2_RAT	-	-	30	GTP-binding protein Rit2
gi|149025066	-	-	29	rCG20598
gi|157822029	-	-	28	SURP and G patch domain containing 2
gi|392348609	-	-	28	Rho guanine nucleotide exchange factor 33-like
gi|149053745	-	-	25	Similar to RIKEN cDNA 0610013E23
gi|149029067	-	-	25	Similar to Ankyrin repeat and IBR domain-containing Protein 1
gi|149048474	-	-	24	rCG41402
gi|392341001	-	-	23	Mitochondrial import inner membrane translocase Subunit Tim23-like
gi|392347937	-	-	20	LOW QUALITY PROTEIN
CEL_RAT	-	-	18	Bile salt-activated lipase
gi|198041672	-	-	17	Trinucleotide repeat-containing gene 6B protein

*The score numbers (score1, 2, and 3) are trial number.

Collagen peptides are in red.

Copyright © 2013 Cognizant Communication Corporation

Figure Legends

Figure 1. The effects of collagenase subtypes on the islet yield, appearance and functions. (A) The islet yield was significantly higher in the GH group (black bar: n=9) compared with the H and G groups. Although no islets were retrieved in the G group (n=9), a substantial number of well-shaped islets were obtained from the H group (white bar: n=9). All values are expressed as the means ± SD. ** $P < 0.01$. **(B)** The proportion of isolated islet size. No significant differences were detected between the GH (black bar: n=9) and H groups (white bar: n=9). **(C)** The blood glucose changes in the transplanted diabetic nude mice were measured. No significant differences were detected between the GH (black line: n=6) and H groups (gray line: n=6). **(D)** The blood glucose changes in the IPGTT were measured. No significant differences were detected between the GH (black line: n=6) and H groups (gray line: n=6).

Figure 2. The effects of sequential injection of different collagenase subtypes on the yield of isolated rat islets. (A) The isolated islet yield in the H→G group (white bar: n=6) was compared with the GH (black bar: n=9) and H (gray bar: n=9) groups. An increase of 20% in the islet yield was seen in the H→G group compared with the H group. **(B)** The isolated islet yield from the G→H group (white bar: n=6) was compared with the GH (black bar: n=9) and G (gray bar: n=9) groups. No beneficial effects were observed after the additional injection of ColH. All values are expressed as the means ± SD. ** $P < 0.01$.

Figure 3. The Plot score distributions in the mass spectroscopic analyses. (A) The search score was plotted for the modification ratio (TMPP-modified peptide/detected peptide ($p<0.05$)). Higher search score indicates higher probability of protein identifications. The highest scored protein (pancreatic lipase) was omitted from the plot. Each analysis is indicated as a different point (●, ▲, and ■). In this plot, putative collagenase substrates can be appeared in the diagonal area (from the origin to

upper right). Col-III and Col-I are indicated by red and green circles, respectively. **(B)** The score distribution of collagens. The plot is demonstrated only for the collagens used in plot (A).

Figure 4. The collagen staining of the pancreatic tissues. The lobular and acinar septa, and the pancreatic ducts in the exocrine tissues were positively stained for Col-I (A), III (C), and VI (D). In these areas, the reaction for anti Col-I and VI was moderate, whereas the reaction for anti-Col-III was well developed. Col-II (B) appeared to be diffusely located in the exocrine tissues. The peri-insular region displayed a weak reaction to Col-II and III (Arrow).

Figure 5. ***In vitro*** **collagen digestion by collagenases.** Collagen digestion was performed for Col-I, II, III, and VI using ColG (left panel) and ColH (right panel). Samples were run in three lanes for each collagen at different sampling times (left: 0 min, middle: 5 min, right: 10 min). The band of collagenase is indicated by a black arrow. The molecular weight was estimated using the marker (M).

Copyright © 2013 Cognizant Communication Corporation

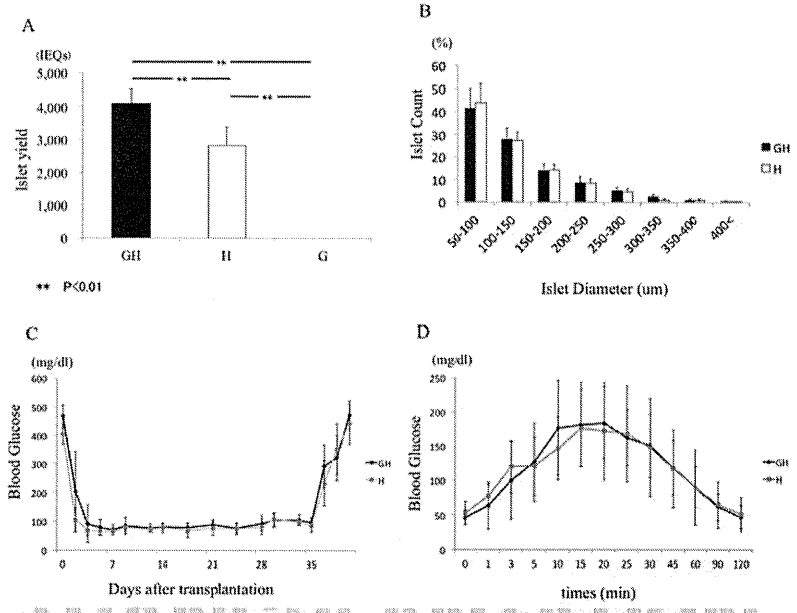

FIGURE 1

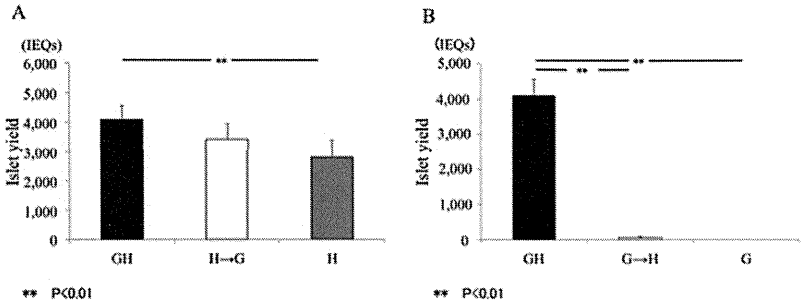

FIGURE 2

Copyright © 2013 Cognizant Communication Corporation

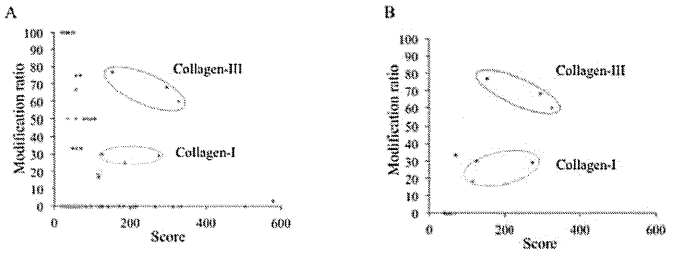

FIGURE 3

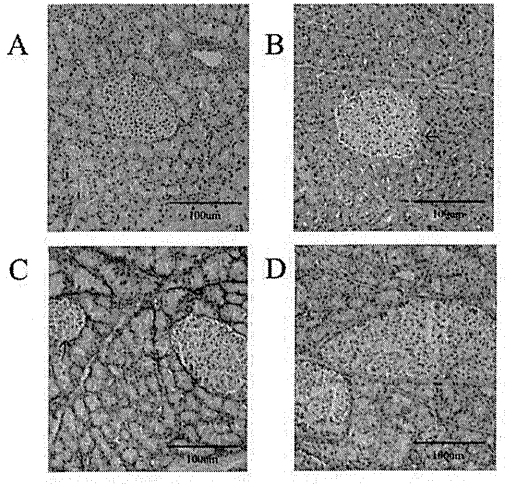

FIGURE 4

Copyright © 2013 Cognizant Communication Corporation

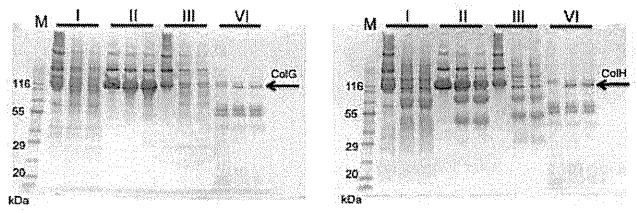

FIGURE 5

Proceedings of ASME 2013 International Mechanical Engineering Congress & Exposition
IMECE2013
November 15–21, 2013, San Diego, California, USA

IMECE2013-63922

CLASSIFICATION OF BLOOD FLOW IN CEREBRAL ANEURYSM CONSIDERING THE PARENT ARTERY CURVES

Toshio Nakayama
Graduate School of Biomedical Engineering, Tohoku University
Sendai, Miyagi, Japan

Shin-ichiro SUGIYAMA
School of Medicine, Tohoku University
Sendai, Miyagi, Japan

Makoto Ohta
Institute of Fluid Science, Tohoku University
Sendai, Miyagi, Japan

ABSTRACT

Background and purpose: Recently, the number of endovascular treatments has increased worldwide because of advances in minimally invasive surgery. We considered the effect of reduced flow due to stent implantation and proposed the design of stent strut pattern from the viewpoint of fluid dynamics. We developed an optimized stent strut pattern using a computational fluid dynamics (CFD) system. A classification of cerebral aneurysms was proposed using the aspect ratio (AR) and the stent strut pattern was optimized. The results of optimal stent strut pattern for reduced blood flow speed and wall shear stress were different, and the influence of the AR values was small because there was no dependence on relationship between blood flow and the AR values due to the use of a straight pipe in the parent artery. The classification of blood flow pattern in a cerebral aneurysm must consider the parent artery curves. In this study, we investigated the relationship between the blood flow pattern in cerebral aneurysms and parent artery curves using CFD.

Methods: To investigate the influence of blood flow based on the parent artery curve, the parent artery shape was constructed as follows. Patient-specific parent artery shape with a cerebral aneurysm was reconstructed using OsiriX. Center line was extracted using a vascular modeling tool kit. The parent artery shape was reconstructed based on this center line using CAD. The diameter of the parent artery was 4 mm. The cerebral aneurysm shape was a combination of a straight pipe and a half sphere, and the AR value was fixed at 1.0. The cerebral aneurysm position varied from the original position to a 180° rotated position.

Tetrahedral numerical mesh was generated with a commercial mesh generator (ICEM CFD 14.0; Ansys Inc.) for the CFD analysis. The numerical blood flow simulation was performed on a supercomputer using the commercial ANSYS FLUENT 6.3 software package and the finite volume method, and a steady flow simulation was performed. Boundary conditions were set for velocity at the inlet, pressure at the outlet, no-slip parent artery, and stent surface. Reynolds numbers at the inlet determined from the mean blood flow speed were 240 and 600.

Results and discussion: In this study, we revealed the blood flow pattern in some cerebral aneurysms using CFD. The pattern in a cerebral aneurysm was influenced by the aneurysm direction and parent artery curves. The blood flow pattern in a neck cerebral aneurysm was classified into two types.

INTRODUCTION

Rupture of a cerebral aneurysm causes massive bleeding in the brain, is life threatening, and has a high probability of brain sequelae. Endovascular treatment with stent implantation in an intracranial artery is one the treatment methods. Stents have become increasingly popular because surgical damage from this treatment appears to be less severe than that from other treatments.

Stents placed in a cerebral aneurysm are thought to reduce blood flow to the aneurysm. The reduction in internal blood flow following stent implantation for a cerebral aneurysm has been investigated by numerical (1-5) and experimental (6, 7) flow studies. To evaluate stenting in this environment, we developed a computational fluid dynamics (CFD) system using a realistic stent and aneurysm (8). As a result, we found that the stent strut pattern has a large effect on reducing blood flow in a cerebral aneurysm. Therefore, we created a methodology to design and optimize stent strut pattern using three-dimensional techniques (9, 10) and proposed several optimized designs.

Ujie et al. proposed that aspect ratio (AR), which is a relationship between height and neck size of the cerebral aneurysm, revealed the relationship between the AR value and aneurysm rupture, and a correlation between the AR value and blood flow pattern in an aneurysm. However, Nakayama et al. demonstrated that all optimized stent strut patterns with different ARs in a straight parent artery were similar because the blood flow was maintained at the aneurysm neck. This result indicates that the blood flow pattern in a cerebral aneurysm is strongly associated with the blood flow pattern in the aneurysm neck, and not with aneurysm geometry. Moreover, Imai et al. used CFD and idealized aneurysm and parent artery shapes to demonstrate the relationship between blood flow and shape. They reported that the blood flow pattern at the aneurysm neck depends on the aneurysm position and the parent artery shape. Therefore, the blood flow pattern in a cerebral aneurysm is strongly affected by aneurysm position and parent artery shape (12, 13).

To verify whether the above hypothesis can be applied to a patient-specific shape, it is necessary to compare flows between a realistic sample and a parent artery aneurysm as well as another realistic sample with the same aneurysm in a different position on the same parent artery. However, it is difficult to collect patient data with the same aneurysm and the same parent artery. Therefore, in this study, a parent artery shape was constructed from a patient-specific artery and an aneurysm with an idealized shape was placed on the artery at different positions. First, we confirmed that the flow pattern in the parent artery was approximately the same as that in the original patient-specific shaped artery.

Consequently, two flow characters were found in the neck that could affect aneurysm flow. Flow patterns in the aneurysm neck were classified into two characters, namely "split" and "side" flows.

MATERIALS AND METHODS

Three-dimensional reconstruction of the parent artery and cerebral aneurysm

The analysis target was the internal carotid–posterior communicating artery junction because this is one of the frequent sites of cerebral aneurysm development. Moreover, only endovascular treatment is available for an aneurysm at this location because it is located deep in the brain and neurosurgery is difficult. All DICOM data were collected at the hospital and transported to us, while maintaining anonymity.

The parent artery shape was constructed to investigate the influence of the parent artery curve on blood flow. First, the patient-specific parent artery shape with cerebral aneurysm was reconstructed using OsiriX. Second, the center line was extracted using the vascular modeling tool kit (15). Finally, the parent artery shape was reconstructed based on this center line using CAD (Rinoceros, Robert McNeel & Associates, USA). Diameter of the parent artery was 4 mm. We reconstructed four parent artery shapes for this study (Figure 1). Here, the inlet length from inlet to proximal of aneurysm was important for reproducing the patient specific blood flow pattern at proximal of aneurysm, this distance was taken for as long as possible.

The blood flow pattern in the aneurysm was affected by aneurysm shape. Therefore, it was necessary to reduce the effect of aneurysm shape. A fixed aneurysm shape was adopted, which was a combination of a straight pipe and a half sphere. AR value was fixed at 1.0. The parent artery and the aneurysm shapes were merged using Rapid Prototyping software (MagicsRP12.1; Materialise, Belgium). The cerebral aneurysm position varied from the original position to a 180° rotated position. Figure 2 shows the realistic parent artery and aneurysm and the reconstructed parent artery shape and the aneurysm in Geometry A. In addition, it shows the relationship between the parent artery and aneurysm position as it is rotated from its original position to 180° rotated position.

Numerical simulation

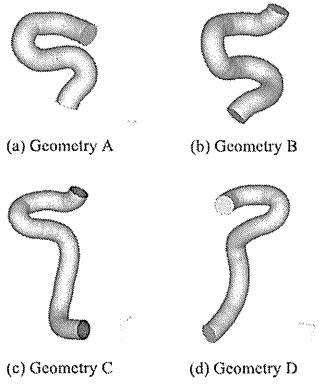

Figure 1 The parent artery shape

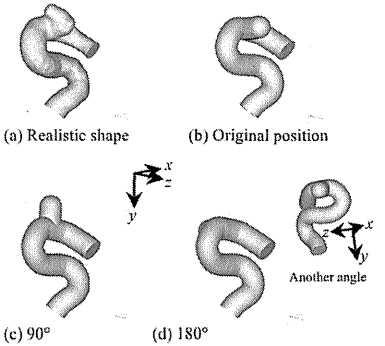

Figure 2 The parent artery shape and aneurysm

Constructed shape data were transferred to a personal computer. A numerical mesh was made using a commercial software package (ICEM CFD 14.0; Ansys Inc., Canonsburg, PA, USA). A tetrahedron was used in the volume mesh, and a prism 3 layer mesh to accurately calculate the blood flow onto the artery's internal surface was used at the artery's internal surface. The mesh number was approximately 300,000–500,000 in all cases.

The constructed mesh data were transferred to a supercomputer at the Institute of Fluid Science (UV; Silicon Graphics Inc., CA, USA). CFD analysis of blood flow was performed using the commercial software package ANSYS Fluent 6.3 (Ansys Inc., Canonsburg, PA, USA) using the finite volume method.

Blood flow was simplified as an isothermal, incompressible, laminar Newtonian flow with a density of 1,050 [kg/m^3] and a viscosity of 0.0035 [Pa s].

The boundary conditions of the inlet, outlet, vessel, aneurysm wall, and stent were time-independent. A flat flow velocity profile of 0.200 and 0.500 [m/s] was introduced at the inlet to maintain consistency with Reynolds numbers of 240 and 600. A constant pressure was set at the outlet. A no-slip condition was employed for the vessel, aneurysm, and stent.

Evaluation method

For evaluation of CFD result, Energy loss, Kinematic energy, and Wall shear stress were used. Energy loss was defined as the power difference from inlet to outlet (17). Kinematic energy was calculated in cerebral aneurysm, Wall shear stress was calculated on cerebral aneurysm.

RESULTS

Figure 3 shows the velocity vectors in the cross-section at the aneurysm center with a Reynolds number of 240. The point of view was toward the distal part from the proximal part of the aneurysm. An inflow zone to the aneurysm is observed in the upper side in the original and 180° cases. The inflow zone is observed in the center of the 90° case.

Figure 4 shows the stream line through the aneurysm neck with a Reynolds number of 240. The colors indicate the speed of blood flow, with blue indicating slower and red indicating faster blood flow. The blue arrow indicates the direction of blood flow. An inflow zone called the bundle of inflow (BOI) (16) was observed at the upper side of the neck in the original position and 180° cases. BOI was observed at the center of the neck in the 90° case. The two BOIs were characterized and named the "side type" and "split type," respectively. Both types were also observed in the other three parent artery shapes.

Figure 5 shows stream lines of the split type with Reynolds numbers
when inle
Figur
Geometry
demonstra
types. In
the neck,
neck. In t

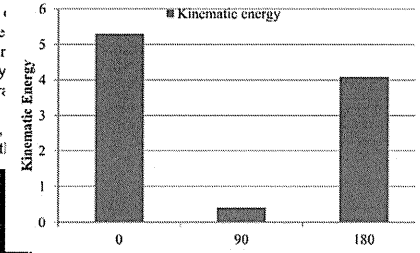

Figure 8 The kinematic energy in cerebral aneurysm

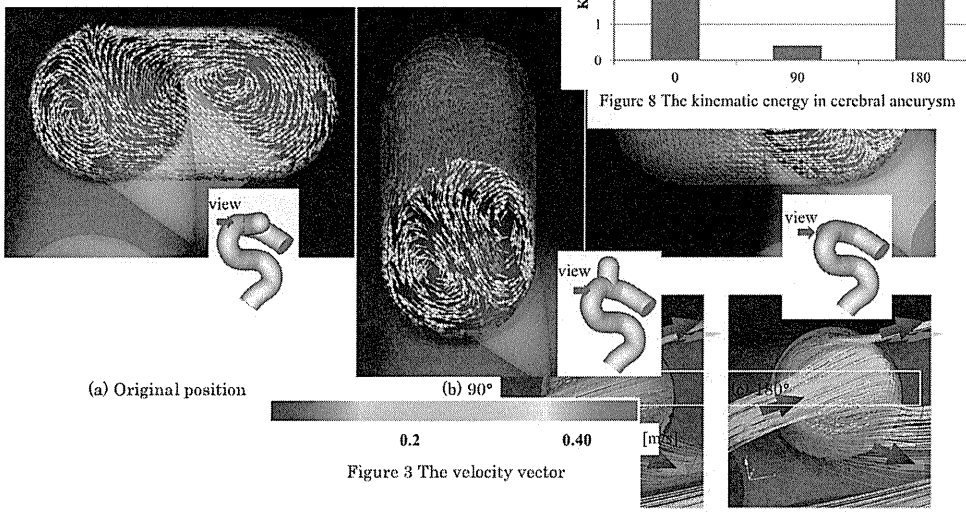

Figure 3 The velocity vector

Figure 5 The stream line (Re = 240 and 600)

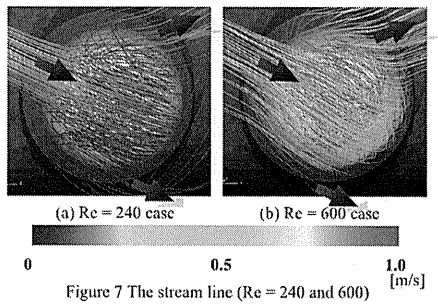

Figure 7 The stream line (Re = 240 and 600)
Geometry D case

the neck, split into two directions, rotated, and flowed out from both sides.

The split type flow pattern was observed in the 90° position of Geometry A, the 135° position of Geometry B, the 90° position of Geometry C, and the 90° position of Geometry D. In common aneurysms, these aneurysm positions are observed in the outer part of the parent artery curvature.

The energy loss is calculated to be 1.96, 1.90, and 1.97 (mW) respectively with 0°, 90°, and 180°. 0° case is control, the difference of the energy loss was 3.1%.

Figure 8 shows the kinematic energy in cerebral aneurysm. The kinematic energy of 90° is the lowest value than another 2 case, and its value is 7% of the control case.

Figure 9 shows the maximum wall shear stress value. The maximum wall shear stress value of 0° is the lowest than another 2 case, and its value is 36% of control case.

DISCUSSION

Our results suggest that the flow pattern in an aneurysm can be classified as "side type" or "split type". Previous studies used an aneurysm on a straight parent artery and the blood flow

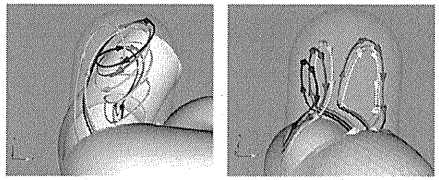

Figure 6 The stream line in an aneurysm (Re = 240)

pattern observed in the aneurysm neck was only the split type. However, when the parent artery curvature was considered, the side type blood flow pattern appeared. These findings have not been characterized because the flow patterns in the neck are dependent on several factors such as parent artery shape, aneurysm shape, and the configuration of the aneurysm and parent artery. Furthermore, it was difficult to study these factors using patient-specific shapes because all shapes are different. Therefore, we reconstructed the parent arteries from the center line and placed an aneurysm with different configurations. Results revealed that the split type only appeared when the cerebral aneurysm position was outside the blood vessel curvature and the side type appeared at other aneurysm positions.

Both flow patterns are described using the position of secondary flow in the parent artery based on the inertial force and the position of the cerebral aneurysm. Imai et al. studied blood flow in the aneurysm neck by investigating both the inflow pattern and inflow flux using a U-tube. Our results were qualitatively consistent with their results.

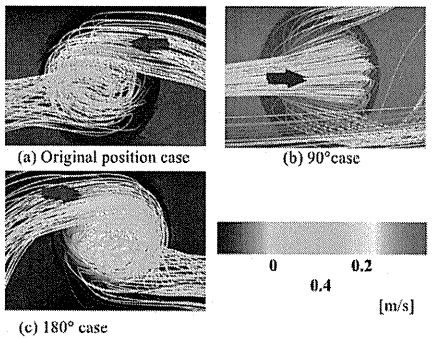

Figure 4 The stream line (Re = 200)

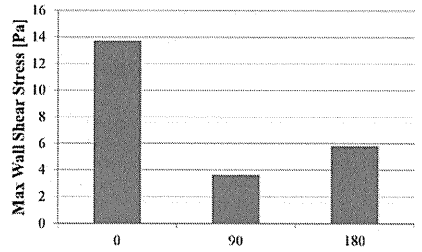

Figure 9 The maximum wall shear stress on aneurysm

Optimizing a cerebral aneurysm stent

In our previous study, we developed and optimized a stent strut pattern (12). The parent artery was a straight pipe, the blood flow pattern was observed in the cerebral aneurysm neck, the inflow to the aneurysm was from the distal neck and outflow to the parent artery was from both sides of the aneurysm neck, which is similar to the "split type" described above.

The side-type flow pattern differs from that in the split type. The split type has one inflow and two outflows, whereas the side type has one inflow and one outflow. Therefore, the side-type flow pattern was not used in that previous stent strut design optimization study. In case of the split type, the blood flow pattern in the aneurysm changed from rotational flow before stent implantation to flow along the aneurysm wall after stent implantation, and the flow of BOI changed from distal to proximal. In case of the side type, the blood flow pattern in the

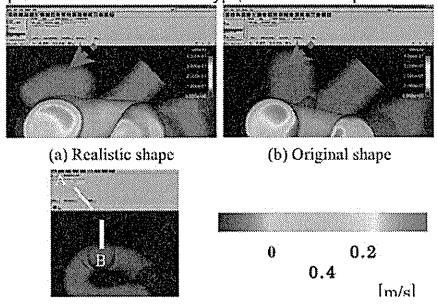

(a) Realistic shape (b) Original shape

(c) Cut-plane position

Figure 10 The velocity contour

aneurysm is rotational before and after stent implantation (8) and the shift in BOI is smaller than that in the split type. Therefore, the change in the flow pattern by stent implantation in the split type is large, whereas it is small in the side type. Blood flow speed in the split type is smaller than that in the side type, because the inertial force of blood flow in the aneurysm neck of the split type is small. The split type is sensitive to the stent strut pattern. The difference in the blood flow pattern is considered to be responsible for the difference in the optimized results of the split type. It was necessary to optimize stent strut pattern for the side type. The split-type flow pattern was symmetrical, whereas the side-type flow was asymmetrical; thus, there is a possibility that the stent strut design would need to drastically change.

Curvature and torsion of the parent artery

In the split type, the inflow zone for the cerebral aneurysm tended to move toward either side with increasing blood flow speed of the parent artery. Figure 7 shows the stream line through the aneurysm neck with Reynolds numbers of 240 and 600. Geometry D shows a strong inflow zone bias. This may be because of the curvature and torsion of the parent artery. The fast blood speed in the cross section after the curvature in a U-shaped pipe is observed outside the pipe due to inertial force. The fast blood speed zone bias was also caused by torsion of the parent artery. Imai et al. reported generating an asymmetric vortex pair in the parent artery with torsion (14). The blood flow pattern in a parent artery with torsion is more complex than that in a parent artery without torsion. The torsion angle of Geometry A was approximately 0°, whereas the torsion angle of Geometry D was >25°. Therefore, information regarding torsion size will be included as a classification parameter.

Comparison of blood flow pattern of realistic and original shapes

Figure 10 shows the velocity contour on some cut planes. The colors indicate the speed of blood flow, blue represents slow and red represents fast. The fast areas of blood flow on Planes A and B were qualitatively consistent. As the blood flow on Plane A is related with the flow into the cerebral aneurysm, the blood flow pattern at the cerebral aneurysm neck was qualitatively consistent. The parent artery constructed in this study reflected the blood flow characteristics of a realistic shape.

Aneurysm position

In this study, the aneurysm was not positioned inside the curvature, and these aneurysms were not treated. Because the curvature of the radius of the internal carotid–posterior communicating artery junction was small, there was no space for an aneurysm inside.

Energy

The energy loss of a whole aneurysm and parent artery, and the kinematic energy were used by the evaluation for blood flow in aneurysm neck. This energy value of split type was observed the lowest than another type. The maximum value of split value was also similar. There is the difference between the split type and the side type from the viewpoint of energy. There is the difference from view point of wall shear stress. Then, it is important that the classification by considering the parent artery curves.

Limitation

In this study, the sidewall-type cerebral aneurysm was analyzed. Thus, an analysis of other predilection sites for the sidewall-type cerebral aneurysm is necessary. We plan to perform a similar analysis on the basilar artery.

Based on position, aneurysms are of two types; the side-wall type occurs at the side of a blood vessel and the end-wall type occurs at the bifurcation of a blood vessel in the cerebral aneurysm. We only used the side-wall type to conduct our CFD analysis. We will analyze the end-wall type and classify the blood flow pattern in the cerebral aneurysm neck.

CONCLUSION

In this study, the blood flow pattern in some cerebral aneurysms was introduced using CFD. The blood flow pattern in a cerebral aneurysm was influenced by the aneurysm direction and parent artery curves. The blood flow pattern in the cerebral aneurysm neck was classified roughly into two types. Considering the parent artery curves, a cerebral aneurysm classification is necessary.

ACKNOWLEDGMENTS

This study was partially supported by a Grant-in-Aid for Scientific Research (C), 24500535, 2012. CFD analysis was performed using the supercomputer at the Institute Fluid Science, Tohoku University.

REFERENCES

1. Aenis, M, Stancampiano, AP, Wakhloo, AK, Lieber, BB. Modeling of flow in a straight stented and nonstented side wall aneurysm model. J Biomech Eng. 1997, 119, 206-212
2. Ohta M, Hirabayashi M, Wetzel S, Lylyk P, Iwata H, Tsutsumi S, Rüfenacht DA. Impact of Stent Design on Intra-Aneurysmal Flow: A computer simulation study. Interventional Neuroradiology, 2004, 10(Supp2), 85-94
3. Ohta M, Wetzel SG, Dantan P, Bachalat C, Lovblad KO, Yilmaz H, Flaud P, Rüfenacht DA. Rheological changes after stenting of a cerebral aneurysm: a finite element modeling approach. Cardiovascular interventional radiology, 2005, 28(6), 768-772
4. Hirabayashi M, Ohta M, Barath K, Rufenacht DA, Chopard B. Numerical analysis of the flow pattern in stented aneurysms and its relation to velocity reduction and stent efficiency. Mathematics and Computers in Simulation, 2006, 72, 128-133
5. Stuhne GR, Steinman DA. Mesh Resolution Requirements for the Numerical Simulation of Flow Through Stented Aneurysms, 2003, Summer Bioengineering Conference
6. Rhee K, Han MH, Cha SH. Changes of flow characteristics by stenting in aneurysm models: influence of aneurysm geometry and stent porosity. Ann Biomed Eng. 2002 vol. 30, 894-904
7. Baráth, Krisztina, Cassot, Francis, Fasel, Jean HD, Ohta M, Rüfenacht DA. Influence of stent properties on the alteration of cerebral intra-aneurysmal haemodynamics: flow quantification in elastic sidewall aneurysm models. Neurological Research, 2005, 27, Vol. 1,120-128
8. Nakayama T, Ohta M, Rüfenacht DA, Takahashi A. Arterial Aneurysm using Realistic Stent Data. C Proceedings of the 6th International Symposium on Advanced Fluid Information. 2006, pp 47-48
9. Nakayama T, Jeong S, Srinivas K, Ohta M. Proceedings the 3rd ASME2010 3rd US-European Fluids Engineering Summer Meeting and 8th International Conference on Nanochannels, Microchannels and Minichannels, Aug.1-5, 2010, pp. FEDSM/ICNMM 2010, 30592
10. Srinivas K, Nakayama T, Ohta M, Obayashi S, Yamaguchi T. Studies on Design Optimization of Coronary Stents, Journal of Medical Devices, 2008, 2, 011004-1-011004-7
11. Ujiie H, Tachibana H, Hiramatsu O, Hazel AL, Matsumoto T, Ogasawara Y, Nakajima H, Hori T, Takakura K, Kajiya F. Effects of size and shape (aspect ratio) on the hemodynamics of saccular aneurysms: a possible index for surgical treatment of intracranial aneurysms. Neurosurgery. 1999 Jul; 45(1):119-29; discussion 129-30
12. Nakayama T, Jeong S, Srinivas K, Ohta M. Effect of the Aspect Ratio of Cerebral Aneurysms on Blood Flow Reduction after Optimized Stent Placement, Proceedings of the 9th International Symposium on Advanced Fluid Information. 2012, pp 424-425
13. Sato K, Imai Y, Ishikawa T, Matsuki N, Yamaguchi T. The importance of parent artery geometry in intra-aneurysmal hemodynamics, Med Eng Phys. 2008 Jul; 30(6): 774-82
14. Imai Y, Sato K, Ishikawa T, Yamaguchi T. Inflow into saccular cerebral aneurysms at arterial bends. Ann Biomed Eng. 2008 Sep; 36(9): 1489-95.
15. http://www.vmtk.org.
16. Anzai H, Nakayama T, Takeshima Y, Ohta M. The Effect of 3D Visualization on Optimal Design for Strut Position of Intracranial Stent. Proceedings the 3rd ASME 2010 3rd US-European Fluids Engineering Summer Meeting and 8th International Conference on Nanochannels, Microchannels and Minichannels, pp. FEDSM/ICNMM 2010, 30591, 2010.
17. Sen Y, Qian Y, Zhang Y, Morgan M. A Comparison of Medical Image Segmentation Methods for Cerebral Aneurysm Computational Hemodynamics. 4th International Conference on Biomedical Engineering and Informatics, 2011 , Vol. 2, 901-904

Genes to Cells

Dmrta1 regulates proneural gene expression downstream of Pax6 in the mammalian telencephalon

Takako Kikkawa[1], Takeshi Obayashi[2], Masanori Takahashi[1,3], Urara Fukuzaki-Dohi[1], Keiko Numayama-Tsuruta[1,4] and Noriko Osumi[1]*

[1]*Division of Developmental Neuroscience, United Centers for Advanced Research and Translational Medicine (ART), Tohoku University Graduate School of Medicine, 2-1, Seiryo-Machi, Aoba-ku, Sendai, Miyagi 980-8575, Japan*
[2]*Division of Applied Informatics for Human and Life Science, Tohoku University Graduate School of Information Science, 6-3-09, Aramaki-Aza-Aoba, Aoba-ku, Sendai, Miyagi 980-8579, Japan*
[3]*Division of Biology, Center for Molecular Medicine, Jichi Medical University, 3311-1, Yakushiji, Shimotsuke, Tochigi 329-0498, Japan*
[4]*Graduate School of Biomedical Engineering, Tohoku University, 6-6-01, Aramaki-Aoba, Aoba-ku, Sendai, Miyagi 980-8579, Japan*

The transcription factor Pax6 balances cell proliferation and neuronal differentiation in the mammalian developing neocortex by regulating the expression of target genes. Using microarray analysis, we observed the down-regulation of *Dmrta1* (*doublesex* and *mab-3*-related transcription factor-like family A1) in the telencephalon of *Pax6* homozygous mutant rats (*rSey*^{2}/*rSey*^{2}). Dmrta1 expression was restricted to the neural stem/progenitor cells of the dorsal telencephalon. Overexpression of *Dmrta1* induced the expression of the proneural gene *Neurogenin2* (*Neurog2*) and conversely repressed *Ascl1* (*Mash1*), a proneural gene expressed in the ventral telencephalon. We found that another Dmrt family molecule, *Dmrt3*, induced Neurog2 expression in the dorsal telencephalon. Our novel findings suggest that dual regulation of proneural genes mediated by Pax6 and Dmrt family members is crucial for cortical neurogenesis.

Introduction

It is essential that a large variety of neuronal cell types are generated at defined times and locations for the development of a functional nervous system. Appropriate patterning of the telencephalon is required for the production of specific sets of neurons (reviewed in Sur & Rubenstein 2005). The embryonic telencephalon is patterned into two major subdivisions, the pallium (cortex) and the subpallium (basal ganglia), with a distinct set of molecules (Puelles *et al.* 2000). Pax6 expression demarcates the dorsal telencephalon (Walther & Gruss 1991) and is crucial for the patterning of the cortex (reviewed in Osumi *et al.* 2008).

Pax6 has another important role in cortical development. Expression of Pax6 is specifically observed in neural progenitor cells in the ventricular zone (VZ). While Pax6 overexpression inhibits proliferation and promotes neurogenesis in the developing cortex (Heins *et al.* 2002), the loss of Pax6 function reduces the size of neural stem/progenitor cell pools in the cortical primordium, indicating that Pax6 can regulate the proliferation of neural stem/progenitor cells in the cortex (Fukuda *et al.* 2000; Estivill-Torrús *et al.* 2002). The level of Pax6 is essential for controlling the balance between the proliferation and differentiation of neuronal progenitors in the cerebral cortex (Sansom *et al.* 2009; Gómez-López *et al.* 2011). These results suggest that Pax6 plays dual roles in promoting cell proliferation and cell differentiation in a highly context-dependent manner.

Multiple functions of Pax6 are mediated by the transcriptional regulation of different target genes. Various genes are reported to be up- or down-regulated in the *Pax6* mutant mouse cortex (Holm *et al.* 2007; Sansom *et al.* 2009). We have previously demonstrated that a gene encoding brain-type fatty acid protein (Fabp7/BLBP), a marker for neural stem cells, is markedly down-regulated in the forebrain and hindbrain of *Pax6* homozygous mutant rats (*rSey*^{2}/*rSey*^{2}) (Arai *et al.* 2005; Numayama-Tsuruta *et al.* 2010). We have shown that Fabp7 is required for the maintenance of proliferating neural stem cells in the developing rat cortex (Arai *et al.* 2005). One of the fucosyltransferase genes, *FucTIX*, is down-regulated in *Pax6* mutant rats; in addition, a neural stem cell marker, LewisX, is synthesized by fucosyltransferase (Shimoda *et al.* 2002). Therefore, Pax6 regulates the expression of a number of molecules to maintain neural stem/progenitor cells.

In contrast, neuronal differentiation is promoted by proneural genes. Specifically, the basic helix-loop-helix (bHLH) transcription factors Neurogenin2 (Neurog2) and Mash1 (Ascl1) regulate neurogenesis and neuronal subtype specification in the telencephalon (Parras *et al.* 2002). Dorsal neural progenitors transiently express Neurog2 (Fode *et al.* 2000), whereas ventral progenitors express Ascl1 (Casarosa *et al.* 1999). In the dorsal telencephalon of the *Pax6* homozygous mutant mouse (*Sey/Sey*) embryo, *Neurog2* expression is down-regulated and *Ascl1* is upregulated (Stoykova *et al.* 2000). A previous study revealed that Pax6 can bind to the enhancer region of *Neurog2*; however, only high concentrations of Pax6 activate this gene in the mouse cortex (Scardigli *et al.* 2003). However, how Pax6 regulates Neurog2 and promotes neurogenesis at the molecular level in the mammalian telencephalon is poorly understood.

In this study, we systematically reanalyzed the transcriptome profiles of wild type (WT) and *rSey*^{2}/*rSey*^{2} rat cortical primordia at the initiation of neurogenesis (Fukuzaki & Osumi 2007). We observed a marked down-regulation of *Dmrta1* (*doublesex* and *mab-3*-related transcription factor-like family A1, *Dmrt4*) in the *rSey*^{2}/*rSey*^{2} rat cortical primordium. The *Dmrt* genes encode a large family of transcription factors involved in sexual development (reviewed by Hong *et al.* 2007). First identified in doublesex of *Drosophila* and MAB-3 of *Caenorhabditis elegans*, the Dmrt family proteins share a DM domain that consists of a highly intertwined zinc finger DNA-binding motif (Erdman & Burtis 1993; Raymond *et al.* 1998). Dmrt family genes are also involved in the development of vertebrate sexual organs. For example, Dmrt1 controls many aspects of testicular development, including the postnatal differentiation of germ cells and Sertoli cells (Raymond *et al.* 2000). Interestingly, *Dmrt3*, *Dmrta1* and *Dmrta2* are expressed in the developing telencephalon (Hong *et al.* 2007; Konno *et al.* 2012). These three Dmrt members have a conserved DMA domain near the C-terminus; however, the role of this DMA domain in biological processes is unclear (Ottolenghi *et al.* 2002). Recent studies have shown that *Xenopus* Dmrta1 and Dmrta2 promote neurogenesis in the olfactory placode (Huang *et al.* 2005; Parlier *et al.* 2013) and that zebrafish Dmrta2 regulates neurogenesis in the telencephalon (Yoshizawa *et al.* 2011). Nevertheless, the precise function of Dmrta1 in the mammalian brain remains largely unknown.

In the developing telencephalon of rat embryos, we uncovered unique Dmrta1 expression patterns and determined that Dmrta1 is regulated by Pax6. Gain-of-function and loss-of-function studies suggested regulatory roles for Pax6, Dmrta1 and proneural bHLH proteins during cortical development. Our findings unveiled dual regulation of *Neurog2* that is mediated by Dmrt family molecules and Pax6; furthermore, this regulation is crucial for regional specification and neurogenesis in the developing cortex.

Results

Genes up- and down-regulated in the Pax6-deficient forebrain

To identify candidate target genes of Pax6, we previously performed transcriptome analyses of WT and *rSey*^{2}/*rSey*^{2} rat telencephalons at E11.5 (corresponding to E9.5 in the mouse) within a day of onset of Pax6 expression using the GeneChip Rat Expression Set 230 2.0 Array, which contains approximately 30 000 probe sets (Fukuzaki & Osumi 2007). In this study, we used the GC content-adjusted robust-multi-array (GC-RMA) algorithm (Wu & Irizarry 2004), which computes expression values from probe intensity values by incorporating probe sequence information.

From this analysis, we identified 35 upregulated and 65 down-regulated genes in the *rSey*^{2}/*rSey*^{2} rat compared with the WT (>1.8-fold change) (Fig. 1A and Table S1 in Supporting Information). The down-regulated genes included *Fabp7*, a previously reported downstream target of Pax6 in the telencephalon of E12.5 *rSey*^{2}/*rSey*^{2} rats (Arai *et al.* 2005). This finding suggests that our screening strategy can identify genes act downstream of Pax6. Other genes showed a marked reduction in expression in the *rSey*^{2}/*rSey*^{2} telencephalon, including *Prr15*, *Map7*, *Dmrta1*, *Sytl2* and *Wnt7a* (Table S1 in Supporting Information). In contrast, upregulated genes showed relatively small fold changes.

Communicated by: Fumio Matsuzaki
**Correspondence:* osumi@med.tohoku.ac.jp

DOI: 10.1111/gtc.12061

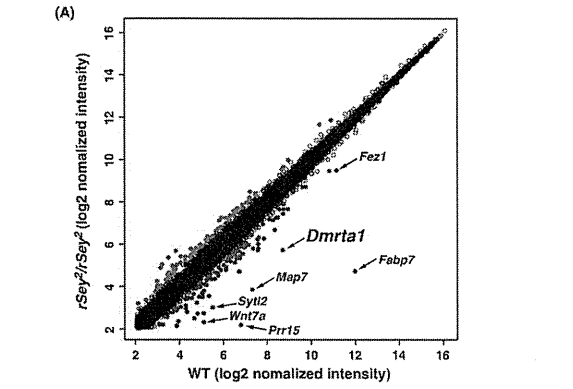

Figure 1 Microarray analysis in the *rSey²/rSey²* rat telencephalon. (A) Scatter plots of gene expression levels in the wild type (*x*-axis) and *rSey²/rSey²* (*y*-axis) rat telencephalon. Dots represent probe sets that are increased (red) or decreased (blue) >1.8-fold in the *rSey²/rSey²* rat telencephalon. (B) Enriched Gene Ontology (GO) terms in genes up- or down-regulated in the *rSey²/rSey²* rat telencephalon. A GO tree obtained from BiNGO shows a hierarchical structure of Gene Ontology Biological Processes, in which the color shading indicates the degree of statistical significance (Benjyamini and Hochberg corrected *P* value <0.01). The number in the circles shows the number of differentially expressed genes in the *rSey²/rSey²* rat (>1.8-fold change). Dmrta1 is assigned to the terms in red circles.

To furthermore understand the identified Pax6-regulated genes in the E11.5 rat telencephalon, we performed a functional assessment using the Gene Ontology Biological Process (GOBP) (Fig. 1B and Table S2 in Supporting Information). One hundred differentially expressed genes in the *rSey²/rSey²* rat (>1.8-fold change) were analyzed using the Gene Ontology (GO) enrichment tool BiNGO package in Cytoscape (Maere *et al.* 2005). The BiNGO-derived graph showed that the genes were mainly assigned to terms involved in 'neurogenesis' (Fig. 1B). This 'neurogenesis' group of genes included *Fabp7*, *Wnt7a*, *Fez1*, *Lrrc4c*, *Rarb* and *Foxa2* (Table S2 in Supporting Information). *Wnt7a* was listed within the top 10 down-regulated genes (Table S1 in Supporting Information). These data are consistent with a previous study that showed decreased *Wnt7a* expression in the telencephalon of the E12.5 *Sey/Sey* mouse (Holm *et al.* 2007). Another study also suggests that Wnt7a is involved in the promotion of neuronal differentiation in the mouse telencephalon (Hirabayashi *et al.* 2004). The subcategory 'embryonic eye morphogenesis' within the GOBP yielded three genes, namely *RARb*, *Aldh1a3* and *Aldh1a1*, with down-regulated expression levels in *rSey²/rSey²* rats (Table S2 in Supporting Information). This finding is not unexpected because our rat forebrain samples at E11.5 contained the eye primordium.

Of the markedly down-regulated genes in *rSey²/rSey²* rats, we focused on *Dmrta1* as a candidate gene regulated by Pax6 because *Dmrta1* encodes a transcription factor that has the potential to regulate the expression of other genes. Furthermore, *Dmrta1* is listed as one of the genes down-regulated in the E12.5 *Sey/Sey* mouse cortex in other transcriptome analyses (Sansom *et al.* 2009; and subsequently Saulnier *et al.* 2012); however, its function was largely unknown when we began our analyses.

Down-regulation of Dmrta1 expression in the telencephalon of developing *rSey²/rSey²* embryos

We examined the developmental sequence of *Dmrta1* expression patterns in WT and *rSey²/rSey²* rat embryos using whole mount *in situ* hybridization (Fig. 2). *Dmrta1* mRNA expression was observed as early as E10.5 in the rat forebrain (Fig. 2A). The expression of *Dmrta1* became markedly restricted to the dorsal telencephalon at E12.5 (Fig. 2C). Consistent with our microarray data, *Dmrta1* mRNA expression was dramatically decreased in the *rSey²/rSey²* telencephalon (Fig. 2F–J).

We next examined the localization of Dmrta1 protein by creating a specific antibody (Fig. S1 in Supporting Information). Dmrta1 protein was specifically observed in the VZ of the dorsal telencephalon overlapping the region expressing Pax6; however, Dmrta1 expression was excluded from the dorsal part of the lateral ganglionic eminence (dLGE) at E12.5 and E14.5 (Fig. 3A–D). Dmrta1 expression was down-regulated in the *rSey²/rSey²* dorsal telencephalon except in the Pax6-negative domain of the medial cortical region (arrows in Fig. 3E,G). These observations indicate that the majority of the neural stem/progenitor cells in the dorsal telencephalon express both Pax6 and Dmrta1 and are regulated by the Pax6-Dmrta1 pathway.

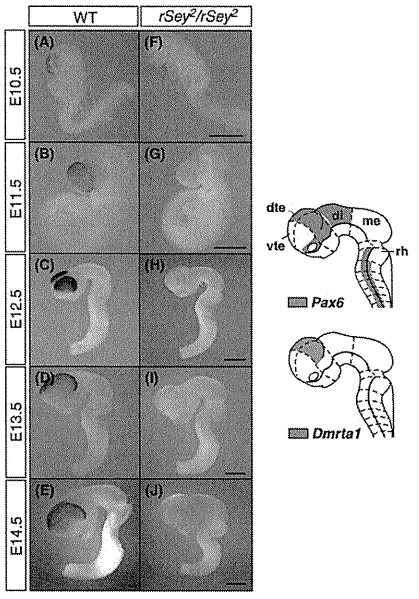

Figure 2 Down-regulation of *Dmrta1* expression in the telencephalon of developing *rSey²/rSey²* embryos. (A–J) Expression patterns of *Dmrta1* mRNA in the wild type (WT) and *rSey²/rSey²* rat brain at E10.5–E14.5. *Dmrta1* mRNA is specifically expressed in the dorsal telencephalon of the WT (A–E), but almost lost in that of the *rSey²/rSey²* (F–J). dte, dorsal telencephalon; di, diencephalon; me, mesencephalon; rh, rhombencephalon; vte, ventral telencephalon. Scale bars represent 1 mm (A–J).

Pax6 can induce Dmrta1 expression

The marked reduction in Dmrta1 expression in the *rSey²/rSey²* rat embryos led us to test whether exogenous *Pax6* can induce *Dmrta1* expression in the developing telencephalon. A *Pax6* expression plasmid was introduced into the ventral telencephalon by electroporation at E11.5. These electroporated embryos were cultured for 30 h using a whole-embryo culture system (Takahashi & Osumi 2010). We found that ectopic Dmrta1 expression was detected in the ventral telencephalon ($n = 3$, Fig. 4). Therefore, Pax6 can induce Dmrta1 expression in the telencephalon.

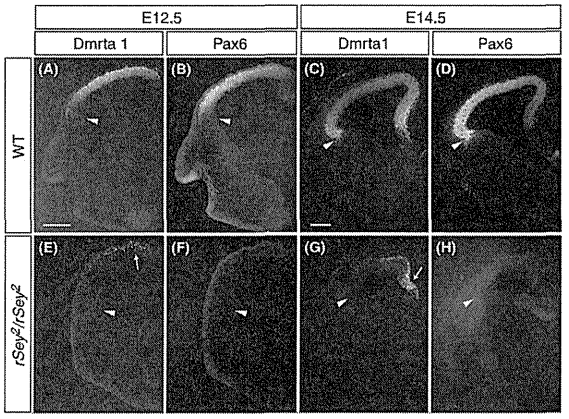

Figure 3 Dmrta1 is expressed in neural stem/progenitor cells of the dorsal telencephalon. (A–H) Localization patterns of Dmrta1 and Pax6 proteins in the wild type (A–D) and *rSey*^{2}/*rSey*^{2} (E–H) telencephalon at E12.5 and E14.5. Arrowheads indicate the position of the pallial/subpallial boundary (PSB). Dmrta1 is highly expressed in the ventricular zone (VZ) of the dorsal telencephalon with a pattern similar to that of Pax6 (A–D) at E12.5 and E14.5. Dmrta1 protein is undetectable in the VZ of the dorsal telencephalon of the *rSey*^{2}/*rSey*^{2} embryo (E, G) with its remaining expression in the medial cortical region at E12.5 and E14.5 (arrows in E, G). Scale bars represent 200 μm (A–H).

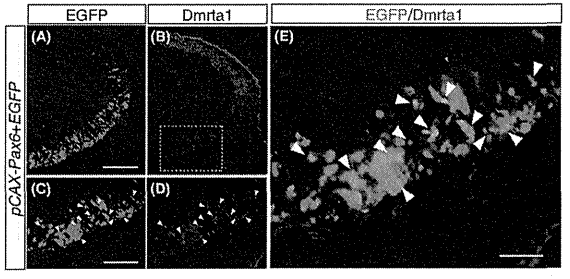

Figure 4 Pax6 can induce Dmrta1 expression. (A–E) *Pax6* and *GFP* expression vectors were transfected into the ventral telencephalic neuroepithelium of wild type rat embryos at E11.5. Dmrta1 expression is ectopically induced in the GFP-positive ventral domain 30 h after electroporation (A and B). Panels (C–E) are magnified views of the boxed area in (B). Dmrta1 is ectopically expressed in GFP-positive cells (arrowheads in C–E). Scale bars represent 100 μm (A–D), 50 μm (E)

Dmrta1 induces Neurog2 expression in the telencephalon

A previous study showed that Dmrta1 is involved in neurogenesis via the regulation of Neurog2 expression in the olfactory epithelium of *Xenopus* embryos (Huang *et al.* 2005). In the cortex, Neurog2 expression was down-regulated in *Sey/Sey* mice (Stoykova *et al.* 2000), and this regulation seems to be directly governed by the binding of Pax6 to the *Neurog2* enhancer (Scardigli *et al.* 2003). These lines of evidence raised the possibility that Dmrta1 regulates the expression of *Neurog2* in parallel with Pax6. Therefore, we examined whether *Dmrta1* is sufficient to induce the expression of Neurog2 in the Pax6-negative telencephalic region (Fig. 5A–E and S2A–D in Supporting Information). The ventral telencephalon of the WT rat embryo was electroporated with expression vectors containing *Dmrta1* and *GFP*. Forty-four hours after electroporation, Neurog2 protein was undetectable in the ventral telencephalon of the non-transfected control side (Fig. 5B) but was ectopically induced in the region transfected with *Dmrta1* (n = 4, Fig. 5C–E). Thus, Dmrta1 induces the expression of Neurog2.

To furthermore investigate whether *Dmrta1* can rescue Neurog2 expression in Pax6-deficient conditions, the dorsal telencephalon of *rSey*^{2}/*rSey*^{2} rat

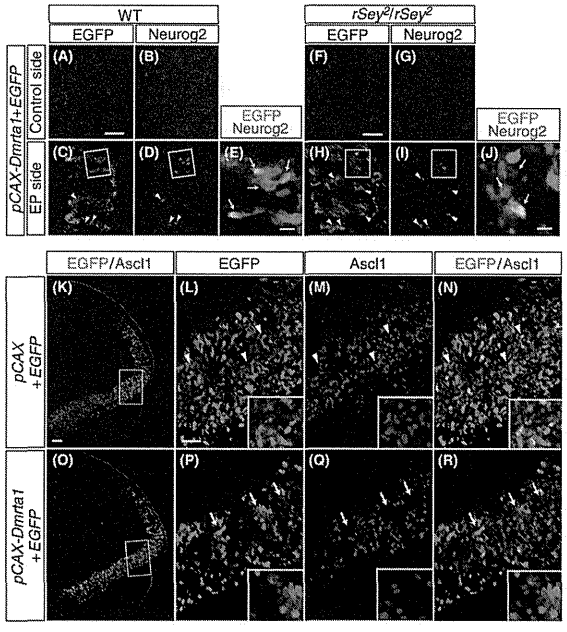

Figure 5 Functions of Dmrta1 in the regulation of proneural genes. (A–J) Induction of Neurog2 expression by Dmrta1. *Dmrta1* and *GFP* expression vectors were transfected into the ventral telencephalic neuroepithelium of the wild type (WT) rat (A–E) and the dorsal telencephalic neuroepithelium of the *rSey*^{2}/*rSey*^{2} rat (F–J) at E11.5, and electroporated embryos were cultured for 44 h. (A–E) Neurog2 expression was ectopically induced in the GFP-positive ventral domain of the WT rat embryos (arrowheads in C, D). Panel (E) is a magnified view of the boxed area in (C, D). Neurog2 was ectopically expressed in GFP-positive cells (arrows in E). (F–J) Neurog2 expression was upregulated in the GFP-positive domain of the *rSey*^{2}/*rSey*^{2} rat embryos (arrowheads in H and I), whereas Neurog2 expression was negative on the control side (F, G). Panel (J) is a magnified view of the boxed area in (H, I). Neurog2 was ectopically expressed in GFP-positive cells (arrows in J). (K–R) Repression of Ascl1 in the ventral domain by exogenous Dmrta1. (K–N) The *GFP* expression vector was introduced into the ventral telencephalic neuroepithelium of the WT rat embryo at E11.5, and electroporated embryos were cultured for 44 h. GFP is detected in the ventral telencephalon (K). (L–N) indicates a magnified view of the boxed area in (K). Ascl1 is normally expressed in the GFP-positive region (arrowheads in L–N). (O–R) Localization patterns of Ascl1 in the embryo electroporated with *Dmrta1* and *GFP* expression vectors. Panels (P–R) show magnified views of the boxed area in (O). Ascl1 expression is repressed in the GFP-positive ventral domain (arrows in P–R). Scale bars represent 50 μm (A–D and F–I), 10 μm (E, J) and 100 μm (K–R).

embryos was electroporated with *Dmrta1* and *GFP* expression vectors at E11.5 (Fig. 5F–J). Forty-four hours after electroporation (Fig. S2E–H in Supporting Information), we detected upregulation of Neurog2 expression in the GFP-positive domain of the *rSey²/rSey²* rat embryos ($n = 3$, Fig. 5H–J), whereas Neurog2 expression was negative on the control side (Fig. 5G). This finding suggests that *Dmrta1* is sufficient to induce Neurog2 expression in the telencephalon in the absence of Pax6.

Dmrta1 represses Ascl1 expression in the telencephalon

Neural stem/progenitor cells in the dorsal telencephalon transiently express Neurog2 (Fode *et al.* 2000). Ventral progenitors express a different bHLH transcription factor known as Ascl1 (Casarosa *et al.* 1999). *Ascl1* expression was ectopically detected in the dorsal telencephalon of *Sey/Sey* mouse (Stoykova *et al.* 2000) and *rSey²/rSey²* rat (T. Kikkawa and N. Osumi, unpublished data) embryos. Therefore, we examined whether Dmrta1 can repress Ascl1 expression in the ventral telencephalon (Fig. 5K–R). Exogenous Dmrta1 that was ectopically expressed in the ventral telencephalon repressed Ascl1 in a cell-autonomous manner ($n = 3$ embryos, Fig. 5O–R). Ascl1 expression was nearly undetectable in cells expressing Dmrta1 (Fig. 5O–R). We counted the number of the total Ascl1$^+$ cells in the VZ of the ventral telencephalon. We found that there was a tendency toward a reduction in the total number of Ascl1$^+$ cells in the embryos that overexpressed Dmrta1 (45.5 ± 6.4, $n = 2$) compared with the control (74.5 ± 13.4, $n = 2$) (T. Kikkawa and N. Osumi, unpublished data). This result may suggest that Dmrta1 directly represses Ascl1 expression without the induction of Neurog2 (see Discussion).

Dmrt family members redundantly regulate Neurog2 expression in the telencephalon

The mouse genome has seven Dmrt family members, and *Dmrt3* and *Dmrta2* are expressed in the dorsal telencephalon of the mouse (Hong *et al.* 2007; Konno *et al.* 2012). Thus, we evaluated the expression of these two genes in E12.5 rat embryos because probes for *Dmrt3* and *Dmrta2* were not included in our original microarray analysis. In the *rSey²/rSey²* rat, *Dmrt3* and *Dmrta1*, but not *Dmrta2*, were down-regulated in the dorsal telencephalon (Fig. 6). The same results were obtained in E12.5 *Sey/Sey* mouse embryos (Saulnier *et al.* 2012). Therefore, *Dmrt3* and *Dmrta1* may be downstream of Pax6 in both the rat and mouse.

We next examined whether *Dmrt3* can regulate Neurog2 expression. We transfected siRNA for *Dmrta1* or *Dmrt3* with a GFP expression vector into the dorsal telencephalon of E11.5 WT rat embryos. The RNAi successfully reduced the expression of Dmrta1 and *Dmrt3* (Fig. S3 in Supporting Information). We counted the number of Neurog2$^+$ cells within GFP$^+$ cells 24 h after electroporation (Fig. 7). The proportion of Neurog2$^+$ cells versus *Dmrta1* siRNA-transfected EGFP$^+$ cells was decreased (2.85 ± 1.21%) compared with a scrambled siRNA against *Dmrta1* (5.20 ± 1.07%) ($n = 4$, Student's *t-test*, $P < 0.05$) (Fig. 7A–H,Q). Knockdown of *Dmrt3* reduced the percentage of Neurog2$^+$ cells (3.79 ± 0.42%) compared with the control group transfected with a scrambled siRNA against *Dmrt3* (6.86 ± 0.98%) ($n = 3$, Student's *t-test*; $P < 0.05$) (Fig. 7I–P,Q). These results suggest that Dmrta1 and Dmrt3 regulate Neurog2 expression in the dorsal telencephalon. There is no difference between the control and *Dmrt* knockdown groups in the number of EGFP$^-$Neurog2$^+$/EGFP$^-$ cells (*Dmrta1*: 6.52 ± 2.37%, Control: 10.20 ± 3.23%, $n = 4$, $P > 0.05$; *Dmrt3*: 8.88 ± 1.30%, Control: 9.39 ± 3.68%, $n = 3$, $P > 0.05$) (Fig. 7R). Therefore, we suggest that Dmrta1 and Dmrt3 induce the expression of Neurog2 in a cell-autonomous manner.

Discussion

Identification of novel genes downstream of Pax6

We have identified genes regulated by Pax6 in the developing telencephalon. The goal of this study was to explore candidate genes that mediate the potent neurogenic function of Pax6. We used rat telencephalons at E11.5 (which corresponds to E9.5 in the mouse), 24 h after the onset of Pax6 expression. In our transcriptome analyses, down-regulated genes in the *rSey²/rSey²* rat exhibited larger fold changes, whereas upregulated genes had relatively small fold changes. Given that Pax6 mainly acts as a transcriptional activator, the down-regulated genes may be directly targeted by Pax6.

The large quantity of information obtained from the GO analyses enabled us to search for interesting features of Pax6 downstream factors. We found transcriptional down-regulation of *Fabp7/BLBP*, *Wnt7a*, *Fez1*, *Lrrc4c*, *Rarb* and *Foxa2*, all of which belong to the 'neurogenesis' GOBP group. We have previously reported that *Fabp7* is essential for the maintenance of neural stem/progenitor cells during early cortical development (Arai *et al.* 2005). Down-regulation of *Wnt7a*, which promotes neuronal differentiation, suggests that impaired Wnt signaling may perturb neurogenesis in early embryonic stages. Fez1 (fasciculation and elongation protein zeta 1) is known to interact with Disc1 (disrupted-in-schizophrenia 1) and regulates neurite outgrowth in PC12 cells (Miyoshi *et al.* 2003); however, the role of Fez1 in mammalian neurogenesis *in vivo* is still unknown. Taken together, it is presumed that Pax6 coordinates the proliferation and differentiation of neural stem/progenitor cells by regulating various genes in a nested manner.

Another markedly down-regulated gene (−2.97) in our transcriptome analyses was *Dmrta1*. This gene has not been identified as a gene downstream of Pax6 in previous studies in *Pax6* mutant rats and mice (Arai *et al.* 2005; Duparc *et al.* 2006) because the probe sets for Dmrta1 were not included in the DNA chips. The expression pattern of Dmrta1 was quite similar to that of Pax6, and Dmrta1 was down-regulated in the telencephalon of both *rSey²/rSey²* rats (Fig. 2) and *Sey/Sey* mice (Saulnier *et al.* 2012). Thus, the Pax6-Dmrta1 pathway is conserved in the developing cortex of both the rat and mouse. Dmrta1 expression was ectopically induced in the ventral telencephalon 30 h after transfection of Pax6, although ectopic expression of *Dmrta1* did not induce Pax6 expression in the ventral telencephalon (Fig. S4 in Supporting Information). Therefore, Dmrta1 is positively regulated by Pax6, but not *vice versa*. We cannot exclude the possibility that the dorsalization of the ventral telencephalon by Pax6 overexpression induces ectopic expression of Dmrta1 in the ventral region. Additional studies are required to elucidate the direct functional interactions between the Pax6 protein and the *Dmrta1* gene.

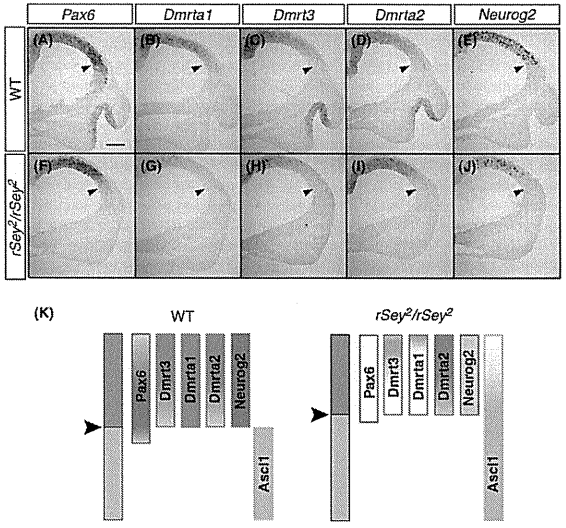

Figure 6 Expression patterns of *Dmrt* family members in the *rSey²/rSey²* rat telencephalon. (A–E) *Dmrta1*, *Dmrt3* and *Dmrta2* are specifically expressed in the dorsal telencephalon with patterns similar to those of *Pax6* and *Neurog2* in the wild type (WT) embryo. (F–J) The expressions of *Dmrta1*, *Dmrt3* and *Neurog2* are down-regulated, while *Dmrta2* expression is maintained in the *rSey²/rSey²* telencephalon. Arrowheads indicate the position of the pallial/subpallial boundary (PSB). (K) Scheme of expression levels of Dmrt family molecules in the WT and *rSey²/rSey²* telencephalon. Ascl1 expression is upregulated in the *rSey²/rSey²* dorsal telencephalon (T. Kikkawa and N. Osumi, unpublished data). Scale bars represent 200 μm (A–H).

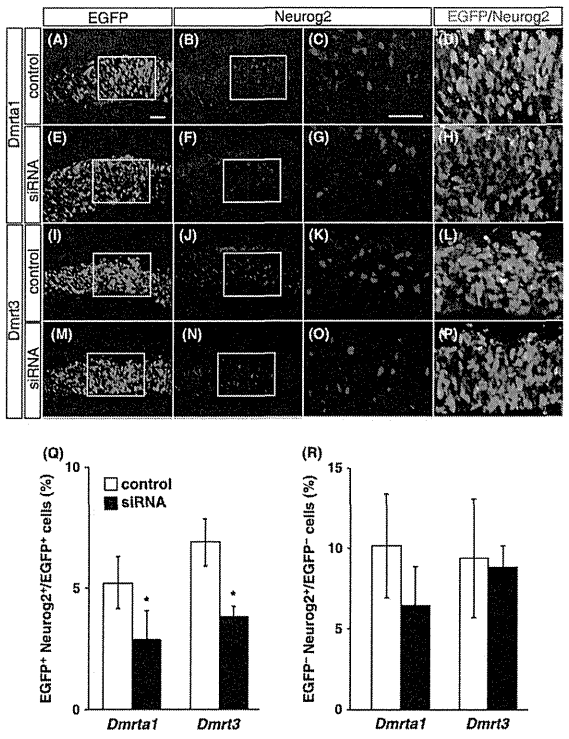

Figure 7 Reduction in Neurog2 expression by knockdown of *Dmrta1* or *Dmrt3* in the telencephalon. (A–Q) siRNA for *Dmrta1* or *Dmrt3* was transfected into the dorsal telencephalon of the wild type rat embryos together with a GFP expression vector at E11.5, and the number of Neurog2$^+$ cells within the GFP$^+$ cells was counted 24 h later. Knockdown of *Dmrta1* reduces the percentage of Neurog2$^+$ cells (2.85 ± 1.21%) compared with the control group (5.20 ± 1.07%) ($n = 4$, Student's t-test, $P < 0.05$) (A–H, Q). Knockdown of *Dmrt3* similarly reduces the percentage of Neurog2$^+$ cells (3.79 ± 0.42%) compared with the control group (6.86 ± 0.98%) ($n = 3$, Student's t-test, $P < 0.05$) (I–P, Q). (R) There is no significant difference in the ratio of EGFP$^-$Neurog2$^+$/EGFP$^-$ between the control (10.20 ± 3.23%) and *Dmrta1* knockdown group (6.52 ± 2.37%) ($n = 4$, Student's t-test, $P > 0.05$). There is also no difference between the control (9.39 ± 3.68%) and *Dmrt3* knockdown groups (8.88 ± 1.30%) ($n = 3$, Student's *t*-test, $P > 0.05$). The scale bar represents 50 μm (A–P).

Dual pathways of Neurog2 regulation by Pax6 and Dmrt family genes

Our experiments show that *Dmrt* genes regulate Neurog2 expression in the telencephalon. Previous studies have shown that Pax6 directly binds to the *Neurog2* enhancer (E1) in the telencephalon and spinal cord (Scardigli *et al.* 2003). However, the E1 element is only active in the lateral domain of the cerebral cortex, where Pax6 is highly expressed (Scardigli *et al.* 2003). Our results indicate that *Dmrta1* is sufficient to induce Neurog2 expression in Pax6-deficient conditions. Additionally, the knockdown of *Dmrta1* or *Dmrt3* causes a reduction in Neurog2 expression in the Pax6-positive dorsal region. Therefore, it is possible that the Dmrt family members redundantly regulate *Neurog2* in addition to the *Pax6-Neurog2* direct pathway (Fig. 8).

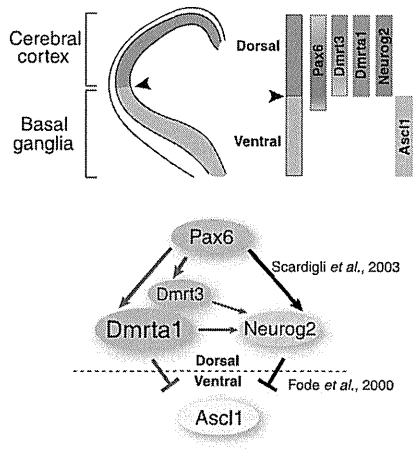

Figure 8 A model of proneural gene regulation by Pax6 and Dmrt family members in the cortical development. Pax6 positively controls expression of another transcription factors *Dmrta1* and *Dmrt3*. Both Dmrta1 and Dmrt3 regulate the expression of a dorsal telencephalon-specific proneural molecule Neurog2. A ventral telencephalon-specific proneural molecule Ascl1 is repressed by both Dmrta1 and Neurog2. Thus, there are dual pathways of proneural gene regulation by Pax6 and Dmrt family members in cortical neurogenesis.

Neurog2 and *Ascl1* are expressed in the dorsal and ventral telencephalon, respectively, and are required to specify the dorso-ventral identity of early-born neurons (Fode *et al.* 2000; Schuurmans *et al.* 2004). Interestingly, *Neurog2* KO mice exhibit upregulation of *Ascl1* in the dorsal telencephalon, indicating that Neurog2 endogenously represses Ascl1 expression in the dorsal telencephalon (Fode *et al.* 2000). We found that Dmrta1 induced the expression of Neurog2 and repressed Ascl1 expression in the telencephalon. The repression of Ascl1 expression was more drastic in the ventral telencephalon compared with Neurog2 induction by Dmrta1, suggesting a possible direct repression of Ascl1. Thus, upregulation of Ascl1 expression in the telencephalon of *rSey*^{2}/*rSey*^{2} rat (T. Kikkawa and N. Osumi, unpublished data) and *Sey/Sey* mouse (Stoykova *et al.* 2000) embryos may be due to the loss of *Dmrt* gene expression.

The consequences of the dual regulation of *Neurog2* mediated by Dmrt family molecules and Pax6 are unclear. There may be a region-specific function to this regulation. Neurog2 is expressed in the cortex, ventral spinal cord, hindbrain and thalamus; furthermore, Neurog2 expression was reduced in these regions in *Pax6* mutant mouse and rat embryos (Stoykova *et al.* 2000; Takahashi & Osumi 2011; Wang *et al.* 2011). Dmrta1 is expressed only in the dorsal telencephalon, suggesting that Dmrta1 may have an important role in the robust regulation of Neurog2 expression in a cortex-specific manner. If Dmrta1 can directly repress Ascl1 expression, it might also reinforce the production of cortex-specific neurons.

The dual regulation of *Neurog2* may provide a time-specific function. Distinct genetic programs operate to specify neuronal identity at different stages of corticogenesis (Schuurmans *et al.* 2004). We found that the expression of Dmrta1 in the dorsal telencephalon reached its peak at the stage when the cortical neurogenesis starts, that is, at E10.5 in the mouse (Konno *et al.* 2012) and at E12.5 in the rat (Fig. 2). On the other hand, the expression of Pax6 continues to later stages. Therefore, Dmrta1 may function to regulate Neurog2 expression at earlier stages of corticogenesis.

Role of Dmrt family members in neurogenesis

Dmrta subfamily members (i.e., Dmrt3, Dmrta1 and Dmrta2) have a common DMA domain, but they do not always have common functions in neurogenesis. *Xenopus* Dmrta1 and Dmrta2 promote neurogenesis in the olfactory placode (Huang *et al.* 2005; Parlier *et al.* 2013), and zebrafish Dmrta2 regulates *Neurog1* in the telencephalon (Yoshizawa *et al.* 2011). The expression of Neurog2 is not altered in *Dmrta2* KO mice, and Dmrta2 maintains neocortical progenitors (Konno *et al.* 2012). Although *Dmrt3* KO mice have no drastic phenotype in the cortex (Konno *et al.* 2012), it is unknown whether the expression of Neurog2 is down-regulated in *Dmrt3* KO mice at the early embryonic stage. We found that the knockdown of *Dmrta1* or *Dmrt3* reduced Neurog2 expression (Fig. 7), suggesting that Dmrta1 and Dmrt3 promote neuronal differentiation via regulation of Neurog2. Therefore, Dmrta1 and Dmrt3 may function differently from Dmrta2 in rodent early corticogenesis. There is a possibility that Dmrta subfamily members have stage-specific functions by interacting with other molecules even though they are structurally similar.

Regarding upstream regulation, expression of *Dmrta1* and *Dmrt3*, but not *Dmrta2*, was down-regu-

lated in *Pax6*-deficient rat embryos (Fig. 6), indicating that Dmrta2 is not regulated by Pax6 in the cortical primordium. Emx2 is another cortex-specific molecule, and *Dmrt3*, but not *Dmrta1* or *Dmrta2*, was down-regulated in *Emx2* mutants (Saulnier *et al.* 2012). All 3 *Dmrt* genes are reduced in *Gli3* mutants, in which the *Wnt* gene expression is severely affected (Hasenpusch-Theil *et al.* 2012; Saulnier *et al.* 2012). *Dmrt3* and *Dmrta2* are suggested to be Wnt target genes in the mouse developing cortex (Hasenpusch-Theil *et al.* 2012; Konno *et al.* 2012). Therefore, *Dmrt3*, *Dmrta1* and *Dmrta2* are all expressed in the developing cortex, but they are differentially regulated by various transcription factors and secreted molecules. Furthermore investigation is necessary to elucidate the precise roles of Dmrta subfamily members in corticogenesis.

Experimental procedures

Animals

Animal experiments were carried out in accordance with the National Institutes of Health guidelines outlined in the Guide for the Care and Use of Laboratory Animals. The Committee for Animal Experimentation of Tohoku University Graduate School of Medicine approved all the experimental procedures described herein. Embryonic day 0.5 (E0.5) was defined as the midday of the day when a vaginal plug was detected. Pregnant Sprague–Dawley (SD) rats were purchased from Charles River in Japan. *Pax6* homozygous mutant rat embryos were obtained by crossing male and female *Small eye* rat heterozygotes (*rSey*^{2}/+) (Osumi *et al.* 1997).

Microarray and GO analysis

Microarray analysis was performed using an Affymetrix rat genome 230 2.0 array as previously described (Arai *et al.* 2005; Fukuzaki & Osumi 2007). Statistical analysis and data visualization were carried out using the R statistical software with Bioconductor packages (R Foundation for statistical Computing, Vienna, Austria, http://www.R-project.org/). GO enrichment analysis was performed using the BiNGO 2.44 plugin (Maere *et al.* 2005) in the Cytoscape 2.8.3 program (Shannon *et al.* 2003). To test for enrichment, a hypergeometric test was conducted, and the Benjamini and Hochberg false-discovery rate was calculated. The network of the enriched categories is presented. Microarray data on gene expression are available with the Gene Expression Omnibus (GEO) accession number GSE43413.

In situ hybridization

In situ hybridization for whole mount embryos and frozen sections was performed as previously described (Osumi *et al.* 1997; Takahashi & Osumi 2002). To obtain templates for the synthesis of riboprobes, cDNA fragments of rat *Dmrta1*, *Dmrt3*, *Dmrta2* were amplified by RT-PCR. The obtained cDNA fragments were cloned into a pGEM-T Easy vector (Promega), pBluescript IISK(-) (Stratagene). The template for rat *Pax6* was used as previously described (Matsuo *et al.* 1993). Rat *Neurog2* (Mizuguchi *et al.* 2001) cDNA was kindly provided by Dr Nakafuku.

Generation of an anti-Dmrta1 antibody

Rat *Dmrta1* (114–1065 bp) was inserted into a pET-28b vector carrying a His_6-tag at the *Nde*1 and *Eco*R1 sites. Recombinant rat Dmrta1 protein was solubilized with 4 M guanidine hydrochloride and then purified with the use of a TALON purification kit (Clontech). The purified protein was emulsified with Freund's complete adjuvant and injected into C57BL6/J mice 3 times at 2-week intervals. After the final immunization, lymphocytes were collected from the spleen and fused with myeloma cells. Briefly, COS-7 cells were transfected with *pCAX-rDmrta1* and then western blots were performed as previously described to check the specificity of the antibody (Sakurai & Osumi 2008).

Immunohistochemistry

Embryos were fixed in 4% paraformaldehyde/phosphate-buffered saline for 2 h. Primary antibodies were diluted with Tris-buffered saline (TBS) containing 0.1% Triton X-100 and 3% bovine serum albumin. The sections were incubated with primary antibodies, including mouse anti-Dmrta1 (1 : 300 or 1 : 50), mouse anti-Ascl1 (1 : 200, 24B7.2D11; BD Bioscience), chicken anti-GFP (1 : 1000; Abcam), rabbit anti-Pax6 (1 : 1000, Inoue *et al.* 2000), rabbit anti-Neurog2 (1 : 5000, Tsunekawa *et al.* 2012), and mouse anti-Neurog2 (1 : 20, 7G4, a gift from Dr D. Anderson, Lo *et al.* 2002). For secondary antibodies, Cy3-conjugated affinity purified anti-rabbit IgG or mouse IgG donkey antibodies (1 : 500; Jackson Immunoresearch Laboratories), and Alexa 488-conjugated affinity purified anti-mouse IgG or chicken IgY goat antibodies (1 : 300; Invitrogen) were used. For observation, sections were mounted with VECTASHIELD mounting medium (Vector Laboratories) and visualized with an LSM5 Pascal (Carl Zeiss) confocal laser-scanning microscope and an Axioplan II fluorescent microscope equipped with an AxioCam CCD camera (Carl Zeiss).

Electroporation into cultured embryos

The method used for electroporation into the telencephalon of E11.5 cultured rat embryos was previously described (Arai *et al.* 2005). To construct the *Dmrta1* expression plasmid, the ORF fragment of RT-PCR-amplified rat *Dmrta1* was inserted into a *pCAX* expression plasmid (Takahashi & Osumi 2002). The *pCAX-mPax6* plasmid (Takahashi & Osumi 2002) or *pCAX-rDmrta1* plasmid was injected into the telencephalon of WT and *rSey*^{2}/*rSey*^{2} rats at E11.5 with *pCAX-EGFP* or *pCAX-nlsEGFP* (Tsunekawa *et al.* 2012) at a 9 : 1 ratio. Immediately, square pulses (50 ms, 70 V, five times) were sent using an electroporator (CUY21; BEX), and the embryos were furthermore cultured for 30 or 44 h. Stealth siRNAs were designed for the 3'UTR sequence of rat *Dmrta1* and *Dmrt3* as follows: *Dmrta1*, 3'-CGACUGUGAGUAGUUUCCUGAGAUU-5'; *Dmrt3*, 3'-ACACUCAUGUUACUCCCGUUCUA AA-5' (Invitrogen). The sequences for scramble control siRNAs were as follows: *Dmrta1*, 3'-CGAAGUGGAUGCUUUAGUCGUCAUU-5'; *Dmrt3*, 3'-ACACAUGUUACUCCCGUUCUCUAAA-5'. siRNA diluted in phosphate-buffered saline at 50 μM was transfected into the E11.5 rat telencephalon with a GFP plasmid, and the embryos were cultured for 24 h.

Statistical analysis

To calculate the number of Neurog2 cells, Neurog2/EGFP-double-positive cells and EGFP-positive cells were counted within a 200 μm × 100 μm area at the ventricular surface of the dorsal telencephalon over five serial cross-sections. Sections were taken from embryos transfected with either control siRNA or siRNA against *Dmrt* family genes (n = 3–4). We also calculated the ratio of EGFP-negative and Neurog2-positive cells to EGFP-negative cells using the same method. The error bars reflect the standard deviation of the mean. Student's t-test was used to determine statistical significance. Values of $P < 0.05$ were considered statistically significant.

Acknowledgements

We would like to thank Drs Yuji Tsunekawa, Daisuke Sakai, Yu Katsuyama and Tadashi Nomura for their technical advice, critical reading and valuable comments. We are grateful to Ms Ayumi Ogasawara, Sayaka Makino, Makiko Hoshino-Sasaki and Emi Ootsuki for their animal care and technical support. We thank all other members of the Osumi laboratory for their valuable comments and discussion. We also thank Dr David J. Anderson for providing antibodies and Dr Masato Nakafuku for providing plasmids. This work was supported by KAKENHI (#17024001 and #22123007 to N.O.) and the Global COE Program 'Basic and Translational Research Center for Global Brain Science' (to N.O.) from MEXT. T.K was supported by Global COE as a Research Associate and by a Research Fellowships of the Japan Society for the Promotion of Science for Young Scientists.

References

Arai, Y., Funatsu, N., Numayama-Tsuruta, K., Nomura, T., Nakamura, S. & Osumi, N. (2005) Role of Fabp7, a downstream gene of Pax6, in the maintenance of neuroepithelial cells during early embryonic development of the rat cortex. *J. Neurosci.* **25**, 9752–9761.

Casarosa, S., Fode, C. & Guillemot, F. (1999) Mash1 regulates neurogenesis in the ventral telencephalon. *Development* **126**, 525–534.

Duparc, R.H., Boutemmine, D., Champagne, M.P., Tetreault, N. & Bernier, G. (2006) Pax6 is required for delta-catenin/neurojugin expression during retinal, cerebellar and cortical development in mice. *Dev. Biol.* **300**, 647–655.

Erdman, S.E. & Burtis, K.C. (1993) The Drosophila double-sex proteins share a novel zinc finger related DNA binding domain. *EMBO J.* **12**, 527–535.

Estivill-Torrús, G., Pearson, H., van Heyningen, V., Price, D.J. & Rashbass, P. (2002) Pax6 is required to regulate the cell cycle and the rate of progression from symmetrical to asymmetrical division in mammalian cortical progenitors. *Development* **129**, 455–466.

Fode, C., Ma, Q., Casarosa, S., Ang, S.L., Anderson, D.J. & Guillemot, F. (2000) A role for neural determination genes in specifying the dorsoventral identity of telencephalic neurons. *Genes Dev.* **14**, 67–80.

Fukuda, T., Kawano, H., Osumi, N., Eto, K. & Kawamura, K. (2000) Histogenesis of the cerebral cortex in rat fetuses with a mutation in the Pax-6 gene. *Brain Res. Dev. Brain Res.* **120**, 65–75.

Fukuzaki, U. & Osumi, N. (2007) The search for downstream target genes of *Pax6* using microassay analysis. In: *Future Medical Engineering Based on Bionanotechnology* (eds M. Esashi), pp. 79–83. London: Imperial College Press.

Gómez-López, S., Wiskow, O., Favaro, R., Nicolis, S.K., Price, D.J., Pollard, S.M. & Smith, A. (2011) Sox2 and Pax6 maintain the proliferative and developmental potential of gliogenic neural stem cells *In vitro*. *Glia* **59**, 1588–1599.

Hasenpusch-Theil, K., Magnani, D., Amaniti, E.M., Han, L., Armstrong, D. & Theil, T. (2012) Transcriptional analysis of Gli3 mutants identifies Wnt target genes in the developing hippocampus. *Cereb. Cortex* **22**, 2878–2893.

Heins, N., Malatesta, P., Cecconi, F., Nakafuku, M., Tucker, K.L., Hack, M.A., Chapouton, P., Barde, Y.A. & Götz, M. (2002) Glial cells generate neurons: the role of the transcription factor Pax6. *Nat. Neurosci.* **5**, 308–315.

Hirabayashi, Y., Itoh, Y., Tabata, H., Nakajima, K., Akiyama, T., Masuyama, N. & Gotoh, Y. (2004) The Wnt/beta-catenin pathway directs neuronal differentiation of cortical neural precursor cells. *Development* **131**, 2791–2801.

Holm, P.C., Mader, M.T., Haubst, N., Wizenmann, A., Sigvardsson, M. & Götz, M. (2007) Loss- and gain-of-function analyses reveal targets of Pax6 in the developing mouse telencephalon. *Mol. Cell. Neurosci.* **34**, 99–119.

Hong, C.S., Park, B.Y. & Saint-Jeannet, J.P. (2007) The function of Dmrt genes in vertebrate development: it is not just about sex. *Dev. Biol.* **310**, 1–9.

Huang, X., Hong, C.S., O'Donnell, M. & Saint-Jeannet, J.P. (2005) The doublesex-related gene, XDmrt4, is required for neurogenesis in the olfactory system. *Proc. Natl Acad. Sci. USA* **102**, 11349–11354.

Inoue, T., Nakamura, S. & Osumi, N. (2000) Fate mapping of the mouse prosencephalic neural plate. *Dev. Biol.* **219**, 373–383.

Konno, D., Iwashita, M., Satoh, Y., Momiyama, A., Abe, T., Kiyonari, H. & Matsuzaki, F. (2012) The mammalian DM domain transcription factor Dmrta2 Is required for early embryonic development of the cerebral cortex. *PLoS One* **7**, e46577.

Lo, L., Dormand, E., Greenwood, A. & Anderson, D.J. (2002) Comparison of the generic neuronal differentiation and neuron subtype specification functions of mammalian achaete-scute and atonal homologs in cultured neural progenitor cells. *Development* **129**, 1553–1567.

Maere, S., Heymans, K. & Kuiper, M. (2005) BiNGO: a Cytoscape plugin to assess overrepresentation of gene ontology categories in biological networks. *Bioinformatics* **21**, 3448–3449.

Matsuo, T., Osumi-Yamashita, N., Noji, S., Ohuchi, H., Koyama, E., Myokai, F., Matsuo, N., Taniguchi, S., Doi, H., Iseki, S., Ninomiya, Y., Fujiwara, M., Watanabe, T., Eto, K. (1993) A mutation in the Pax-6 gene in rat small eye is associated with impaired migration of midbrain crest cells. *Nat. Genet.* **3**, 299–304.

Miyoshi, K., Honda, A., Baba, K., Taniguchi, M., Oono, K., Fujita, T., Kuroda, S., Katayama, T. & Tohyama, M. (2003) Disrupted-In-Schizophrenia 1, a candidate gene for schizophrenia, participates in neurite outgrowth. *Mol. Psychiatry* **8**, 685–694.

Mizuguchi, R., Sugimori, M., Takebayashi, H., Kosako, H., Nagao, M., Yoshida, S., Nabeshima, Y., Shimamura, K. & Nakafuku, M. (2001) Combinatorial roles of olig2 and neurogenin2 in the coordinated induction of pan-neuronal and subtype-specific properties of motoneurons. *Neuron* **31**, 757–771.

Numayama-Tsuruta, K., Arai, Y., Takahashi, M., Sasaki-Hoshino, M., Funatsu, N., Nakamura, S. & Osumi, N. (2010) Downstream genes of Pax6 revealed by comprehensive transcriptome profiling in the developing rat hindbrain. *BMC Dev. Biol.* **10**, 6.

Osumi, N., Hirota, A., Ohuchi, H., Nakafuku, M., Iimura, T., Kuratani, S., Fujiwara, M., Noji, S. & Eto, K. (1997) Pax-6 is involved in the specification of hindbrain motor neuron subtype. *Development* **124**, 2961–2972.

Osumi, N., Shinohara, H., Numayama-Tsuruta, K. & Maekawa, M. (2008) Concise review: Pax6 transcription factor contributes to both embryonic and adult neurogenesis as a multifunctional regulator. *Stem Cells* **26**, 1663–1672.

Ottolenghi, C., Fellous, M., Barbieri, M. & McElreavey, K. (2002) Novel paralogy relations among human chromosomes support a link between the phylogeny of doublesex-related genes and the evolution of sex determination. *Genomics* **79**, 333–343.

Parlier, D., Moers, V., Van Campenhout, C., Preillon, J., Leclere, L., Saulnier, A., Sirakov, M., Busengdal, H., Kricha, S., Marine, J.C., Rentzsch, F. & Bellefroid, E.J. (2013) The Xenopus doublesex-related gene Dmrt5 is required for olfactory placode neurogenesis. *Dev. Biol.* **373**, 39–52.

Parras, C.M., Schuurmans, C., Scardigli, R., Kim, J., Anderson, D.J. & Guillemot, F. (2002) Divergent functions of the proneural genes Mash1 and Ngn2 in the specification of neuronal subtype identity. *Genes Dev.* **16**, 324–338.

Puelles, L., Kuwana, E., Puelles, E., Bulfone, A., Shimamura, K., Keleher, J., Smiga, S. & Rubenstein, J.L. (2000) Pallial and subpallial derivatives in the embryonic chick and mouse telencephalon, traced by the expression of the genes Dlx-2, Emx-1, Nkx-2.1, Pax-6, and Tbr-1. *J. Comp. Neurol.* **424**, 409–438.

Raymond, C.S., Murphy, M.W., O'Sullivan, M.G., Bardwell, V.J. & Zarkower, D. (2000) Dmrt1, a gene related to worm and fly sexual regulators, is required for mammalian testis differentiation. *Genes Dev.* **14**, 2587–2595.

Raymond, C.S., Shamu, C.E., Shen, M.M., Seifert, K.J., Hirsch, B., Hodgkin, J. & Zarkower, D. (1998) Evidence for evolutionary conservation of sex-determining genes. *Nature* **391**, 691–695.

Sakurai, K. & Osumi, N. (2008) The neurogenesis-controlling factor, Pax6, inhibits proliferation and promotes maturation in murine astrocytes. *J. Neurosci.* **28**, 4604–4612.

Sansom, S.N., Griffiths, D.S., Faedo, A., Kleinjan, D.J., Ruan, Y., Smith, J., van Heyningen, V., Rubenstein, J.L. & Livesey, F.J. (2009) The level of the transcription factor Pax6 is essential for controlling the balance between neural stem cell self-renewal and neurogenesis. *PLoS Genet.* **5**, e1000511.

Saulnier, A., Keruzore, M., De Clercq, S., *et al.* (2012) The doublesex homolog Dmrt5 is required for the development of the caudomedial cerebral cortex in mammals. *Cereb. Cortex*. doi:10.1093/cercor/bhs234.

Scardigli, R., Baumer, N., Gruss, P., Guillemot, F. & Le Roux, I. (2003) Direct and concentration-dependent regulation of the proneural gene Neurogenin2 by Pax6. *Development* **130**, 3269–3281.

Schuurmans, C., Armant, O., Nieto, M., *et al.* (2004) Sequential phases of cortical specification involve Neurogenin-dependent and -independent pathways. *EMBO J.* **23**, 2892–2902.

Shannon, P., Markiel, A., Ozier, O., Baliga, N.S., Wang, J.T., Ramage, D., Amin, N., Schwikowski, B. & Ideker, T. (2003) Cytoscape: a software environment for integrated models of biomolecular interaction networks. *Genome Res.* **13**, 2498–2504.

Shimoda, Y., Tajima, Y., Osanai, T., Katsume, A., Kohara, M., Kudo, T., Narimatsu, H., Takashima, N., Ishii, Y., Nakamura, S., Osumi, N. & Sanai, Y. (2002) Pax6 controls the expression of Lewis x epitope in the embryonic forebrain by regulating alpha 1,3-fucosyltransferase IX expression. *J. Biol. Chem.* **277**, 2033–2039.

Stoykova, A., Treichel, D., Hallonet, M. & Gruss, P. (2000) Pax6 modulates the dorsoventral patterning of the mammalian telencephalon. *J. Neurosci.* **20**, 8042–8050.

Sur, M. & Rubenstein, J.L. (2005) Patterning and plasticity of the cerebral cortex. *Science* **310**, 805–810.

Takahashi, M. & Osumi, N. (2002) Pax6 regulates specification of ventral neurone subtypes in the hindbrain by establishing progenitor domains. *Development* **129**, 1327–1338.

Takahashi, M. & Osumi, N. (2010) The method of rodent whole embryo culture using the rotator-type bottle culture system. *J. Vis. Exp.* **42**, e2170.

Takahashi, M. & Osumi, N. (2011) Pax6 regulates boundary-cell specification in the rat hindbrain. *Mech. Dev.* **128**, 289–302.

Tsunekawa, Y., Britto, J.M., Takahashi, M., Polleux, F., Tan, S.S. & Osumi, N. (2012) Cyclin D2 in the basal process of neural progenitors is linked to non-equivalent cell fates. *EMBO J.* **31**, 1879–1892.

Walther, C. & Gruss, P. (1991) Pax-6, a murine paired box gene, is expressed in the developing CNS. *Development* **113**, 1435–1449.

Wang, L., Bluske, K.K., Dickel, L.K. & Nakagawa, Y. (2011) Basal progenitor cells in the embryonic mouse thalamus - their molecular characterization and the role of neurogenins and Pax6. *Neural Dev.* **6**, 35.

Wu, Z. & Irizarry, R.A. (2004) Preprocessing of oligonucleotide array data. *Nat. Biotechnol.* **22**, 656–658; author reply 658.

Yoshizawa, A., Nakahara, Y., Izawa, T., Ishitani, T., Tsutsumi, M., Kuroiwa, A., Itoh, M. & Kikuchi, Y. (2011) Zebrafish Dmrta2 regulates neurogenesis in the telencephalon. *Genes Cells* **16**, 1097–1109.

Received: 7 February 2013
Accepted: 1 April 2013

Supporting Information

Additional Supporting Information may be found in the online version of this article at the publisher's web site:

Figure S1 Generation of an anti-Dmrta1 antibody.

Figure S2 Overexpression of *Dmrta1* and *GFP* expression vectors in the rat telencephalon.

Figure S3 Effects of siRNA for *Dmrta1* and *Dmrt3* in the rat telencephalon.

Figure S4 Dmrta1 cannot induce the expression of Pax6 in the ventral telencephalon.

Table S1 Down- and upregulated genes in *rSey2/rSey2* rat telencephalon

Table S2 Enriched GO terms in genes down- and upregulated in the *rSey2/rSey2* rat telencephalon

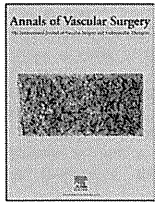

Evaluation of spinal cord ischemia with a retrievable stent graft is useful for determining the type of repair for a case of patch aneurysm

Junetsu Akasaka, MD, PhD Kei Takase, MD, PhD Koichi Tabayashi, MD, PhD

PII: S0890-5096(13)00656-0

DOI: 10.1016/j.avsg.2013.08.024

Reference: AVSG 1820

To appear in: *Annals of Vascular Surgery*

Received Date: 8 April 2013

Revised Date: 9 August 2013

Accepted Date: 25 August 2013

Please cite this article as: Akasaka J, Takase K, Tabayashi K, Evaluation of spinal cord ischemia with a retrievable stent graft is useful for determining the type of repair for a case of patch aneurysm, *Annals of Vascular Surgery* (2014), doi: 10.1016/j.avsg.2013.08.024.

Evaluation of spinal cord ischemia with a retrievable stent graft is useful for determining the type of repair for a case of patch aneurysm

Junetsu Akasaka, MD, PhD[1)], Kei Takase, MD, PhD[2)], Koichi Tabayashi, MD, PhD[3)]

1) Division of Cardiovascular Surgery, Tokyo Medical University Hachioji Medical Center, Tokyo, Japan

2) Division of Radiology, Tohoku University Graduate School of Medicine, Sendai, Japan

3) Tohoku Kosei-Nenkin Hospital, Sendai, Japan

Corresponding author:

Junetsu Akasaka, MD, PhD

Division of Cardiovascular Surgery

Tokyo Medical University Hachioji Medical Center

1163 Tate-machi, Hachioji, Tokyo 185-8991, Japan

E-mail: junc_ak@hotmail.com